



# Cloud radar observations of multi-scale variability of cloud vertical structure associated with Indian summer monsoon over a tropical location

Patra Sukanya<sup>1,2</sup> · M. C. R. Kalapureddy<sup>1,2</sup>

Received: 28 February 2020 / Accepted: 2 November 2020 / Published online: 23 January 2021  
© Springer-Verlag GmbH Germany, part of Springer Nature 2021

## Abstract

Tropics nurture three different types of convective clouds, i.e., shallow cumulus, cumulus congestus, and deep cumulonimbus. The vertical structure of clouds holds a crucial metric in studying tropical clouds. Ground-based high-resolution cloud radar measurements are the potential candidate in exploring the characteristics of various types of tropical clouds and their evolution. Quality-controlled cloud radar data containing a total of five million vertical profiles of equivalent reflectivity factor (VPR) are used to examine the intra-seasonal variation of cloud vertical structure (VSC) during the Indian summer monsoon (ISM) over Mandhardev (18.04° N, 73.87° E, and ~ 1.3 km AMSL) in the Indian Western Ghats. The cumulus congestus (Cc) in the transition of shallow to deep clouds is investigated for the first time using the hourly VPR data for 60 consecutive ISM days. Mid-level moistening plays a vital role in this non-precipitating shallow to precipitating congestus transformation and increment of the rain accumulation. Low cloud reflectivity distribution can distinguish precipitating and non-precipitating clouds that help to classify the observed monsoon as normal or below normal. More than 150 mm of rain accumulation during ISM is associated with more than 22% of high clouds. This particular aspect indicates that cold rain processes are essential to assess the ISM over the observational site. FFT analysis on the time series of low-, mid-, and high-level cloud regions with the VPR shows prominent intra-seasonal variability of 5–10, 10–20, and 30–60 days periodicities. This study highlights the significance of VSC over tropics pertinent to the monsoon large scale atmospheric condition.

**Keywords** Indian summer monsoon · Tropical cloud vertical structure · Cloud radar · Vertical profile of reflectivity factor · Tri-modal convection · Mid-level moistening

## 1 Introduction

Clouds are crucial in the Earth's energy balance, hydrological cycle, climate change predictions (Wielicki et al. 1995) and in weather forecasting (Tiedtke 1989) via radiative effects, latent heat release, and precipitation. Earth radiation budget critically depends on cloud morphological properties (like cloud occurrence altitude, geometrical depth, cloud spatial distribution) and microphysical properties (like cloud particle phase, shape, and size, ice water path, liquid water

path, optical thickness; Sassen and Wang 2008). Changes in cloud amount affect the large-scale atmospheric circulation by modifying the radiative and latent heating of the atmosphere (Slingo and Slingo 1988; Randall et al. 1989; Stephens 2005). However, the cloud's genesis shows differences with the change in latitude, mainly due to the variation of solar energy received by the Earth's surface. The atmospheric response of precipitating cloud systems and the rainfall during monsoon season at tropics depend on the vertical structure of the cloud as it is associated with the heat source (e.g., Webster et al. 1998; Devasthale and Grassl 2009; Devasthale and Fueglistaler 2010). Therefore, quantitative investigation of the cloud vertical structure, both spatially and temporally, can give an insight on microphysical processes during different stages of the cloud lifecycle, which can improve our understanding of the cloud feedback mechanism in the climate system (Wang et al. 2000; Gao et al. 2014).

✉ M. C. R. Kalapureddy  
kalapureddy1@gmail.com

<sup>1</sup> Indian Institute of Tropical Meteorology (IITM), Dr. Homi Bhabha Road, Pashan, Pune 411008, India

<sup>2</sup> Atmospheric and Space Science Division, Savitribai Phule Pune University, Pune 411007, India

Convective clouds over the tropics are of three different types: shallow cumulus, moderate cumulus congestus, and deep cumulonimbus cloud (e.g., Johnson et al. 1999). Thus, the study of the vertical structure of tropical clouds is essential in understanding different cloud types and the processes involved in their genesis, evolution, and precipitation. The realistic representation of tropical convection in the atmospheric models is a long-standing grand challenge for numerical weather forecasts and global climate predictions (Moncrieff et al. 2012). Compared to the extra-tropical atmosphere, the clouds over the tropical atmosphere are poorly understood. A better understanding of the cloud-scale physical processes that affect cloud lifetime requires high-resolution measurements in clouds (Brenguier and Wood 2009). Profiling cloud radar observations complemented by other passive and active remote sensors are now continuously available from ground-based observational networks. Vertically pointing cloud radars can provide excellent height and temporal resolution observations of clouds (e.g., Kollas et al. 2007). The cloud vertical structure (VSC) from cloud radars observed vertical profiles of equivalent reflectivity factor (VPR) provides a complete picture than in-situ measurements, facilitating the better interpretation of cloud processes. Therefore, investigation on macro and microphysical characteristics and the evolution of tropical clouds using VPR measurements are of utmost importance.

Indian monsoon (ISM), a vital part of the Asian monsoon system, is one of the most dominant tropical circulation systems in the general circulation of the atmosphere (Goswami 2005). More than 80% of the yearly ISM rainfall is received during the southwest monsoon season from June to September (Rajeevan et al. 2013). Characteristics of ISM are determined by seasonal changes in atmospheric circulation and precipitation produced by the asymmetric heating of land and sea. Synoptic scale lows and depressions are the primary sources of rain over the Indian monsoon region, which in general, is called low-pressure systems. Due to the quasi-periodic intra-seasonal variability of the ISM, over the Indian territory, there exists “active” and “break” phases of ISM rainfall (Krishnamurti and Bhalme 1976; Gadgil 2003). This intra-seasonal variability of ISM (30–60 days oscillation) is associated with the northward propagation of the tropical convergence zone (e.g., Sikka and Gadgil 1980), which represents the ascending branch of the regional Hadley circulation. It further causes enhanced (decreased) rainfall over central and western India and decreased (increased) rainfall over the southeastern peninsula and eastern India (e.g., Krishnan et al. 2000), and hence it is named as active (break) phases of ISM. During the active and break ISM spells, central India and western India show similar features. One of the outstanding features of ISM is the two coastally oriented narrow rainfall maxima, one along the Western Ghats (WG) and the other along the Myanmar Coast. An

extensive research work on south Asian monsoon region (India and adjoining oceans) using climatological TRMM data, has shown that the coastal regions of western India, WG, and western Myanmar are the regions of heavy precipitation (e.g., Romatschke and Houze 2011) resulted out of the interaction between the northward propagating intra-seasonal oscillations and the shallow orography in the two regions (Rao 1976). The renewed interest in ISM high rainfall studies can be seen over the Indian West Coast region (e.g., Francis and Gadgil 2006; Choudhury et al. 2018). A recent ground-based radar study on the vertical structure of convective storms during monsoon focuses on precipitation features over the WG (Utsav et al. 2019). Therefore, it can be concluded that most research efforts over the WGs were mainly confined to the investigation of orographic rainfall and their inter-annual variability. However, a detailed and systematic study on clouds that ultimately produce rain lacks due to the lack of high-resolution cloud sensitive observations. Since rain is the final product of precipitating clouds, huge chances lie in passing over properties of different types of clouds or the conditions favorable for rain when focusing only on rain study. On the other hand, cloud radar obtained VSC is a much efficient parameter to understand the non-precipitating to precipitate cloud systems and favorable spatio-temporal conditions in producing rain compared to the surface-based rain measurement. Hence, in this work, based on the availability of high-resolution observations from Ka-band radar, VSC has been studied to explore different types of cloud, their genesis, and macro-physical properties associated with the intra-seasonal variation of ISM.

Earlier statistical studies ISM relied on climatological datasets (spanning ten or more years) owing to coarse temporal resolution observations. The advantage of the present study lies in the availability of more than five million profiles in 5 years of high height-time resolution radar measurements, which helps advance our understanding of monsoon clouds from the cloud turbulence scale to intra-seasonal scales. The availability of such a copious amount of radar data also helps determine the interaction of different time scales and variability of cloud vertical structure with better statistical significance. In this study, we analyze cloud evolution spanning the entire day, followed by day-to-day progressions extending to a monthly scale and then extending it for three consecutive monsoon years. Diurnal cloud evolution helps in understanding the mechanism behind the formation of shallow and deep convective clouds. A few consecutive days of cloud evolution is then analyzed and is related to large scale circulation over the study domain. On the other hand, an hourly scale analysis of VPR for month duration was carried to explain the transformation of shallow cloud into cumulus congestus and then deep convection. Thanks to the cloud radar technology for the first time, it enables the VSC parameter from the VPR. The proposed cloud vertical

structure is a new parameter to characterize the large scale ISM, which otherwise widely done to date mostly with surface rain measurements that is the last stage of a cloud. This study uses solely high-resolution VPR, which is the proxy for cloud vertical structure. Thus, it is a potential but straightforward technique for evaluating the influence and vigor of ISM well in advance by characterizing the cloud system over any location in India during the ISM. Therefore the VSC parameter helps to understand pertinent background conditions that lead to the end product, ISM rainfall. Information on VSC can potentially impact the monsoon studies for better predictability skills, which infers cloud and rain processes. These processes are involved with the transformation of non-precipitating to precipitating cloud systems, which can be studied by VSC's evolution.

## 2 The system, data, and methodology

This study uses vertical looking millimeter-wavelength cloud radar reflectivity-factor profile (VPR) measurements of Ka-band scanning polarimetric radar (KaSPR) operating at 35.29 GHz. KaSPR has been providing high resolution (25 m and 1 s) measurements of cloud and precipitation over Mandhardev (18.04° N, 73.87° E, and ~1.3 km AMSL) Western Ghats region of India from a mobile platform since June 2013. KaSPR has the Doppler capability to measure the radial velocity. Doppler weather radar measured radial velocity in the vertical looking mode infers the vertical speed of cloud particles, which are influenced by background atmospheric wind when those cloud particles are relatively small in size. However, the zenith looking radial velocity infers only downward fall velocity (−ve) of hydrometeor (based on the size of cloud ice or cloud droplet particle or raindrop) under the precipitation sensitive conditions.

Besides, dBZ<sub>e</sub>, Doppler capability of cloud radar measured vertical velocity is also used to infer the size of the drops using Gunn and Kinzer (1949). Further details of the KaSPR operation in zenith FFT mode can be found in KaSPR technical document (2012). KaSPR operates under a hybrid scan strategy (cyclic volume scan, range height indicator scan, and vertical looking) to study 3-D cloud structures and vertical pointing observations for 5 min duration at every 15 min interval are available. KaSPR possesses sensitivity of ~ −45 dBZ<sub>e</sub> at 5 km and is therefore sensitive to the cloud droplet. Cloud radars, especially 35 GHz, are susceptible to airborne water bodies' viz. hydrometeors (cloud particles and raindrops) or biological targets called biota. To segregate the biota contribution from the radar reflectivity (Z<sub>e</sub>) factor measurements, an indigenously developed quality control TEST algorithm (Kalapureddy et al. 2018) is used to confirm genuine cloud measurements by screening out the noise and non-meteorological biota information.

In brief, the TEST algorithm uses theoretical noise equivalent curves to filter out the receiver noise floor. Based on a four-point running average and standard deviation of Z<sub>e</sub> at each height level, it can distinguish biota and cloud droplets depending on their small and long correlation period (i.e., large and lower standard deviation), respectively. Therefore, usage of the TEST algorithm confirms pure cloud measurements by screening out the noise and non-meteorological information (Fig. 12c; Kalapureddy et al. 2018). There exists significant attenuation due to gases (mainly water vapor) and precipitation, especially at the millimeter-wave cloud radars. It is straighter forward to tackle with water vapor attenuation using local weather and climate information by using atmospheric thermodynamical profiles with the standard millimeter-wave propagation model. However, the challenge comes more with the precipitation attenuation, which is more dynamic in nature. The challenge is mainly because of the complexity associated with the verity of the precipitation process due to its vertical and horizontal aerial extent and the cloud macro- and micro-physical associated cloud dynamics. Therefore, precipitation attenuation needs to invoke accordingly based on the dynamic conditions of precipitation precisely. The necessary gaseous correction to VPR is incorporated with the radar equation, and radar calibration and validation aspect has been taken care of using CloudSat comparison (Sukanya and Kalapureddy 2019). It is safe to use KaSPR data during the drizzle cases where both rainfalls are less than 3 mm h<sup>−1</sup> and the maximum drop size confines below 2.5 mm. With dynamically invoked precipitation attenuation corrections, this limit can be extended only below moderate rain conditions of less than 10 mm h<sup>−1</sup> with raindrop size distribution tail confine well below 4 mm drop sizes. Since Mie scattering correction at Ka-band due to heavy rain is more effective above 30 dBZ<sub>e</sub>, those heavy rain cases are mostly not considered for this work. Moreover, in the statistical analysis, the contribution of those high Z<sub>e</sub> value cases (~ 5000 profiles) is negligible compared to the total number of cases per month (more than one lakh profiles).

This study uses 3 years (2013–2015) VPR measurements of KaSPR around the Indian summer monsoon (ISM) season (JJAS). High-resolution quality-controlled measurements of cloud radar can provide more than ten thousand profiles each day. Likewise, for each month, more than lakh profiles, and for 3 years, a total of five million profiles analyzed. Indian Standard Time (IST) is used in this study where IST = UTC + 5:30 h; whereas local mean solar time (LT) = IST + 0.067 × (82.5-longitude of a location in India) hours.

The other complementary data sets available over or near the radar site, Optical Rain Gauge (ORG), and Vaisala DigiCORA RadioSounde System (GPS-RS) are also used to complement this study. Optical Rain Gauge (Optical

Scientific, OSi, USA) is a precipitation gauge and can measure rain and snow accurately in almost all weather conditions, rain rate, and water equivalent accumulation in any adverse environment with a temporal resolution of every minute. GPS-RS data is taken from high altitude cloud physics laboratory in Mahabaleshwar, which is radially at a distance of at ~26 km towards south of the radar. GPS-RS provides upper air profiles of pressure, temperature, and relative humidity measurement along with GPS based wind information. Other complementary data is from ERA-Interim ( $0.125^\circ \times 0.125^\circ$ ), TRMM ( $0.5^\circ \times 0.5^\circ$ ), IMD ( $1^\circ \times 1^\circ$ ) and GPCP ( $1^\circ \times 1^\circ$ ) gridded data. In this study, TRMM-3G31 latent heating profiles are used to complement the KaSPR observed different types of clouds. 3G31 is gridded data of resolution  $0.5^\circ \times 0.5^\circ$  and is averaged over a region from  $72.5^\circ$  to  $75^\circ$  E and  $17^\circ$  to  $19^\circ$  N. ERA-Interim relative humidity (RH) and u and v component of wind profiles used for different pressure levels at  $0.125^\circ \times 0.125^\circ$  spatial resolution with a time resolution of 6 h over radar site. ERA-interim is used to decipher the large-scale background condition parallel to the evolution of cloud vertical structure observed from cloud radar, in terms of relative humidity (RH) and also horizontal wind speed and direction.

Further, ERA-Interim specific humidity and horizontal wind are utilized to estimate horizontal moisture advection profiles. RH anomaly is computed using ten years of the climatological mean. Both RH and wind information is used during Jul and Aug 2015 to investigate the reason for the transformation of shallow cloud to cumulus congestus and congestus to the deep cloud. In this study, GPCP: daily precipitation ( $\text{mm day}^{-1}$ ) product used version v1.2. This daily rainfall data averaged over the region from  $73.5^\circ$ – $74.5^\circ$  N and  $17.5^\circ$ – $18.5^\circ$  E is used to compute monthly mean rainfall by averaging all the daily rainfall values for that 1 month.

According to the tri-modal distribution (Johnson et al. 1999), three types of clouds are evident over tropics, namely shallow cumulus, cumulus congestus, and deep convective cloud, as shown in Fig. 1. These three estate types of cloud distribution are adopted in this study as a primary building block representing 3 years of monsoon convection using cloud radar data. In addition to these three convective cloud types, three other layered cloud types also included in this work, namely double-layered cloud, multi-layered cloud, and cirrus cloud. Besides the TEST algorithm that helps provide accurate height information of a cloud, a separate cloud class algorithm was developed to classify these six types of cloud depending on their base (CB) and top (CT). Unless otherwise stated, the vertical profiles' observational height is above the ground level (AGL) of KaSPR, which needs to add 1.35 km to infer it above the mean sea level (AMSL). The VPR comprises height information from 0.9 to 16.5 km AGL. There exist ~640 range bins with the VPR. More than 70–80% range bins of VPR contain cloud

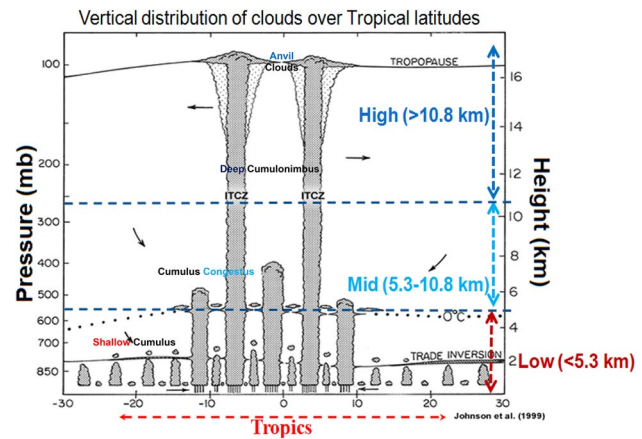


**Fig. 1** Vertical distribution of convective clouds over tropical latitudes for the meridional distribution of shallow cumulus, cumulus congestus, and deep cumulonimbus across the tropics. Source Figure: Johnson et al. (1999). Further, the macro (micro)-physical subdivision levels/estates are namely low (warm), mid (mixed) and high (ice)-cloud regions. Two overlays dashed lines correspond to the altitude at 0° and  $-40^\circ\text{C}$  over the Western Ghats

information continuously from 0.9 to 10 km altitude, which is a continuous VSC; generally, continuous VSC saw during the deep cloud.

The cloud classification algorithm tracks to identify the cloud top and base information utilizing the VPR height-level data, and based on it, the type of cloud has categorized as follow:

- a. Shallow cloud:  $\text{CT} < 3 \text{ km}$ .
- b. Cumulus congestus:  $\text{CB} < 3 \text{ km}$   $\text{CT} > 5 \text{ km}$  and  $\text{CT} < 8 \text{ km}$ .
- c. Deep cloud:  $\text{CB} < 3 \text{ km}$  and  $\text{CT} > 8.5 \text{ km}$ .
- d. Cirrus cloud:  $\text{CB} > 10 \text{ km}$  and  $\text{CT} > 10.8 \text{ km}$ .
- e. Double layered cloud: shallow cloud ( $\text{CT} < 3 \text{ km}$ ) and cirrus cloud ( $\text{CB} > 10 \text{ km}$  and  $\text{CT} > 10.8 \text{ km}$ ).

We mainly consider low-level shallow cloud and high-level cirrus cloud as a double-layered cloud. Due to the influence of ISM circulation by the low-level westerly jet and upper-level easterly jet, this double-layered cloud is one of the dominant ISM cloud features.

There has been considered another genre when no cloud is present in the whole vertical column of the atmosphere and named as 'no cloud' regime. We mainly consider low-level shallow cloud and high-level cirrus cloud as double-layered cloud since it is the feature of those days having a minimal amount of rainfall, beside the fact that this kind of double-layered clouds is more dominant than the shallow cloud and any other mid-level cloud (altocumulus) in terms of the duration. Generally, most of the time, when the mid level cloud is present, shallow low cloud and high cirrus

cloud are also there making it another category as a multi-layered cloud which we did not include in this paper as we could not find any connection of multi-layered cloud with different background monsoon condition.

The duration of these cloud types estimated from the number of profiles over which the cloud part sustained as each profile represents 1 s. Times, when there is no cloud signature in the complete VPR, are termed as ‘no cloud’ regime was also considered. Based on this cloud classification, Table 1 is prepared to summarize the quantitative information on VSC for 3 years of KaSPR data.

Besides these three convective types, the cloud has also classified according to its phase as clouds below 0° isotherm consist of only water drops, clouds existing below the temperature -40 °C consisting of ice particles alone, and cloud existence between 0° isotherm and -40 °C containing both supercooled water droplets and ice particles. It has been seen from the temperature profile of the 2 years (2012–2013) of GPS-RS data over the radar site, the 0° isotherm and -40 °C corresponds to the height of 5.3 km

and 10.8 km AMSL respectively. Hence clouds are classified as warm cloud regions (< 5.3 km), mixed-phase cloud region (> 5.3 km and < 10.8 km), and ice cloud region (> 10.8 km). Classification of this type helps to understand the importance of different cloud types, their evolution, which finally contributes to decipher the underlying processes producing them.

To see the evolution of VSC two pair of cases having contrasting VSC and background are considered in this study; (1) when there is a presence of deep cloud (top > 12 km AMSL) and presence of only shallow cloud (top < 3 km AMSL), (2) presence of low-pressure system (23–24 Aug 2014) around 15°–20° E and 70°–75° N which can be considered as the close vicinity of radar site and presence of high-pressure system (27–28 July 2015) over the Bay of Bengal. The first pair of cases is taken on 09 Sep and 31 Jul, 2015. For the second pair of cases, background condition is ensured from the IMD daily chart, and that condition is also established in the result part using ERA-interim RH and horizontal wind direction datasets.

**Table 1** Cloud type quantification using VPR for the three consecutive ISMs during 2013–2015

	No cloud	CT < 3 km		Cumulus congestus		Deep cloud		Cirrus		Double layered	
		Duration (%)	dBZe	Duration (%)	dBZe	Duration (%)	dBZe	Duration (%)	dBZe	Duration (%)	dBZe
<b>2013</b>											
May	68.99	–	41.63	7.47	–	26.01	5.88	–	0	–	32.22 15.31
June	60.79	–	34.71	17.61	–	19.73	8.14	9.87	4.73	–	29.43 22.53
Sept	39.10	–	34.18	30.87	–	12.92	2.65	16.13	9.56	–	26.24 29.92
Oct	70.60	–	31.92	21.18	–	7.25	2.77	17.37	1.73	–	28.06 16.78
<b>2014</b>											
May	73.47	–	39.46	6.65	–	18.91	3.60	5.52	5.44	–	28.29 11.85
June	57.55	–	33.27	32.11	–	20.20	6.16	11.14	4.07	–	30.35 18.05
July	30.32	–	35.06	39.50	–	19.41	13.11	5.98	9.25	–	30.48 33.87
Aug	12.64	–	38.04	65.58	–	16.94	8.62	10.39	12.14	–	30.01 50.50
<b>2015</b>											
June	65.94	–	36.20	21.01	–	21.45	2.70	19.90	3.35	–	28.47 21.37
July	48.66	–	34.47	45.96	–	17.54	6.38	–	0	–	28.90 32.99
Aug	30.44	–	39.14	64.78	–	21.81	3.89	10.75	2.49	–	29.46 34.4
Sept	49.09	–	35.75	20.55	–	11.94	3.80	15.43	6.52	–	29.78 32.29

### 3 Cloud evolution based on their contrasting vertical structure and the associated background conditions

The diurnal cycle of contrasting cloud vertical structure is evaluated using VPR in Figs. 2 and 4 on 09 Sep and 31 Jul, 2015. The number of vertical profiles is almost similar on these 2 days, but the dominance of different types of clouds, i.e., deep and shallow convective clouds respectively, creates the contrast between them. Figure 2a depicts the height-time-intensity (HTI) map of VPR measurements of KaSPR on 09 Sep 2015, which reveals the presence of tall, vigorous, deep convective clouds existing for more than half a day. In addition to the presence of deep clouds, the rest of the day comprises of non-precipitating cloud ( $Z_e < -20 \text{ dBZ}_e$ ) at either low- or mid-levels. The

gradient in the  $Z_e$  value in Fig. 2a around 5 km AMSL indicates the presence of the radar bright-band. Such gradients in  $Z_e$  further suggests phase change of ice particles to water drops as they cross the  $0^\circ$  isotherms (melting level). This transition of phase about the melting layer is evident from the simultaneous vertical velocity profile measurements (Fig. 2d). Wide range variability of weaker  $Z_e$  values just above the melting level (Fig. 2a), with a near-constant weak fall velocity (Fig. 2d), confirms the smaller ice particles. Though cloud height is maintained ( $> 10 \text{ km}$ ) for more than half a day, the maximum rain rate (Fig. 2h) corresponds to the period spanning 5 h, when the radar  $Z_e$  value shows enhancement ( $\sim 20 \text{ dBZ}_e$ ) at the lower warmer region. The rain event near 13:20 IST starts with a heavy drizzle (rain rate  $> 1 \text{ mm h}^{-1}$ ), which later converts into the rain after 14:00 IST. Whenever  $Z_e$  value in the ice phase region (marked by the black square box) increases, the rain rate also increases.

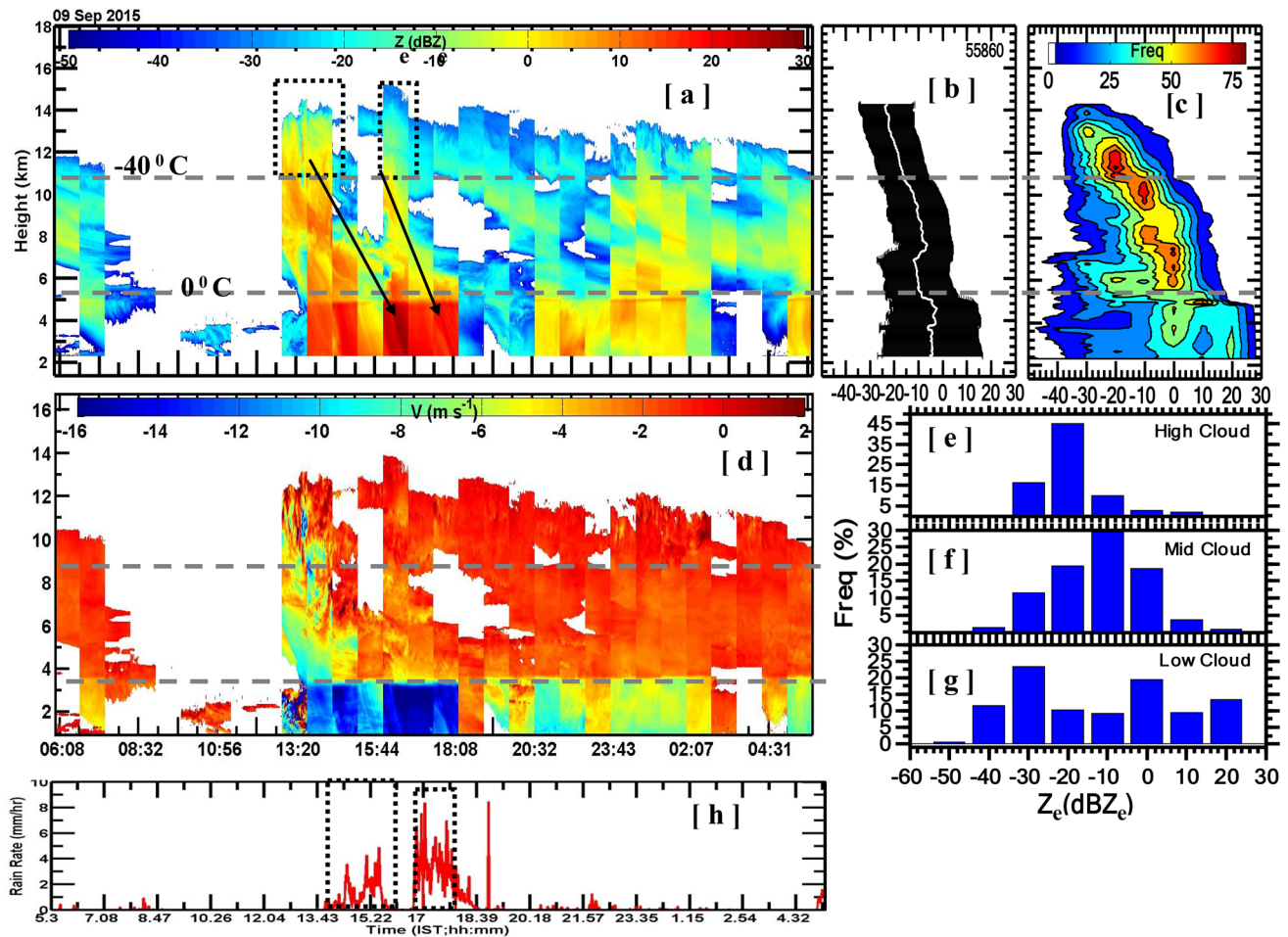


**Fig. 2** Complete evolution of the vertical structure of deep convective cloud shown with **a** height-time-intensity (HTI) map of cloud radar measured  $Z_e$ , **b** mean VPR with standard deviation, **c** CFAD analysis of  $Z_e$ , **d** HTI map of cloud radar measured vertical velocity, **e–g** histogram analysis of  $Z$  for low-, mid- and high-level clouds, and **h**

surface rain rate measurement from ORG on 09 Sep 2015. Two overlays dashed lines correspond to the altitude at  $0^\circ$  and  $-40^\circ \text{C}$  over the Western Ghats. The arrows show the gradual increase of  $\text{dBZ}_e$  at a low level just after the enhanced  $\text{dBZ}_e$  value at the ice phase region

reaches a maximum ( $\sim 10 \text{ dBZ}_e$ ), rain episodes can observe in the warm cloud region. Most of the time, the  $Z_e$  value crosses  $5 \text{ dBZ}_e$  in the ice phase region. Therefore, it may be concluded that the ice growth process plays a vital role in increasing the rain rate. Rain intensity is also confirmed from the vertical velocity measurements below the bright band (Fig. 2d). Wherever the vertical velocity exceeds  $-6.5 \text{ m s}^{-1}$ , they represent raindrops of size 1 mm (Gunn and Kinzer 1949). Mean VPR enlightens on the mean vertical profiles of cloud particle size or its number density. Mean VPR (white line in Fig. 2b) representing a typical deep cloud event shows the same rate at the warm phase cloud (below 5 km) region due to the presence of uniform cloud particles, converted into the rain. Wide variability ( $\pm \sim 20 \text{ dBZ}_e$ ) in the standard deviation of  $Z_e$  in the same region is caused due to cloud droplet to raindrop transition, and initiation and dissipation phase of deep cloud.

Contour Frequency by Altitude Diagram (CFAD) indicates the frequency of the  $Z_e$  profile and hence, the cloud at each altitude. CFAD analysis in Fig. 2c shows that more than 50% (yellow color) of ice crystals can grow bigger particles to descend from the ice phase region to the mixed-phase cloud region. Further, 40% (green color) among the ice particles is converted into bigger ice particles (probably at the expense of supercooled water droplets) to reach the warm phase region and fall as rain droplets. The presence of cloud particles in the three different cloud phase region can be seen from histogram analysis in Fig. 2e–g. In the warm region, bi-modal distribution peaks at  $-30$ , and  $0 \text{ dBZ}_e$  indicate non-precipitating and drizzling clouds (Liu et al. 2008). Further, the presence of a moderate amount of high drizzling cloud is evident from the secondary peak at  $20 \text{ dBZ}_e$  (Fig. 2g).

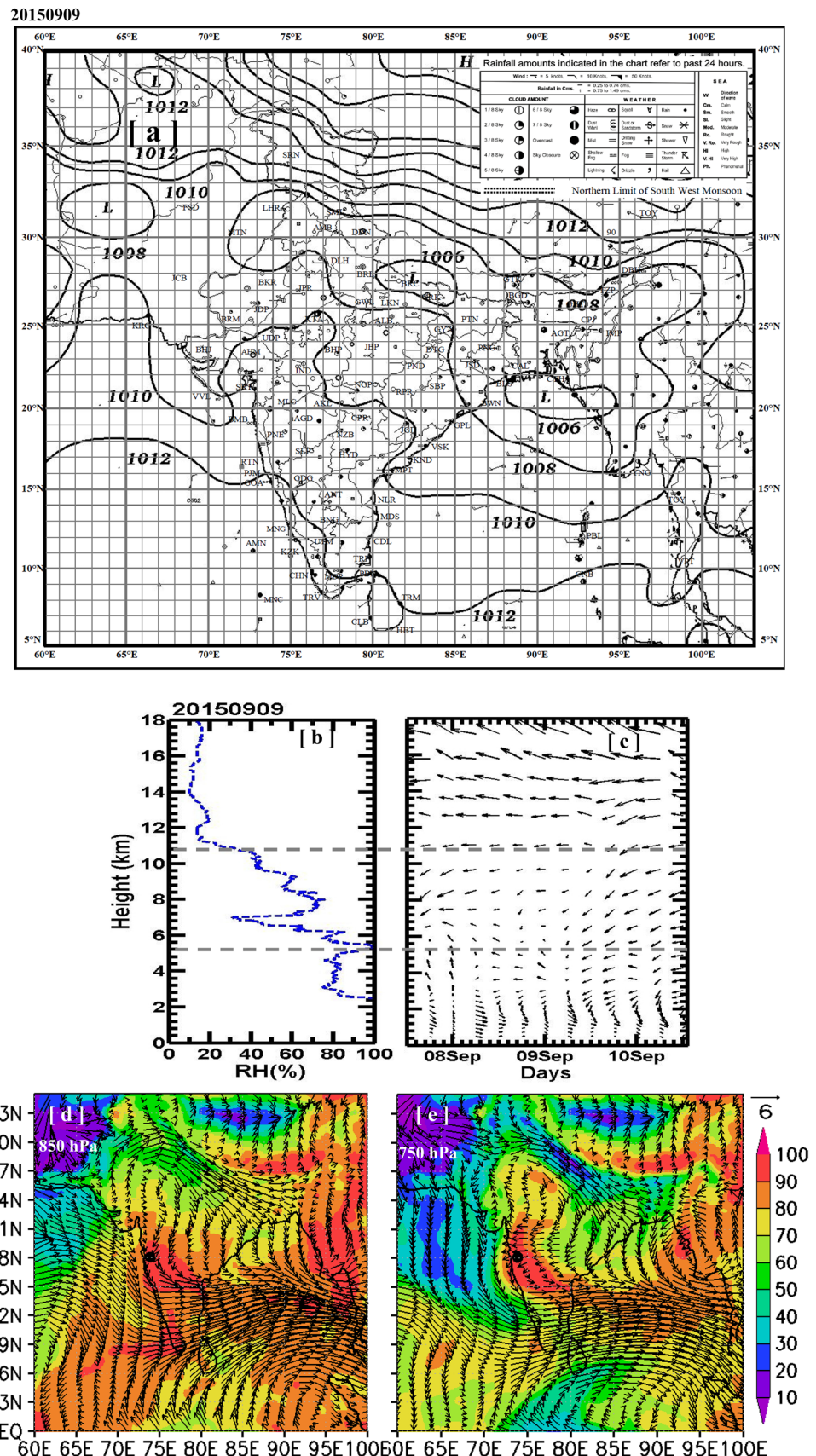
The large-scale background conditions investigated using the IMD weather map from the daily weather report, RH from GPS-RS, wind direction from ERA-reanalysis data (3 days period, with the analysis day at center) are depicted in Fig. 3a–c, respectively. Low wind speed over radar site is evident from widely spread isobars over radar site in the daily weather report in Fig. 3a. Despite a weak low-pressure region over the Bay of Bengal and foothills of Himalaya, moisture convergence is sufficient to form a deep cloud over the radar site. RH profile in Fig. 3b also supports this fact as it is more than 80% (60%) up-to 6 (10) km AMSL. Figure 3c mid-level wind shows less speed (within the square box) than the low levels, which results in less vertical shear in the mid-level. The absence of vertical wind shear and adequate humidity ( $> 60\%$ ) at the mid-level, helps in cloud growth. Figure 3d, e represents the horizontal cross-section of RH at 850 and 750 hPa with horizontal wind speed and direction superimposed. From Fig. 3, the presence of cyclonic motion at 850 and 750 hPa over the coastal part of the Arabian Sea is evident, which brings moisture-rich winds over the radar

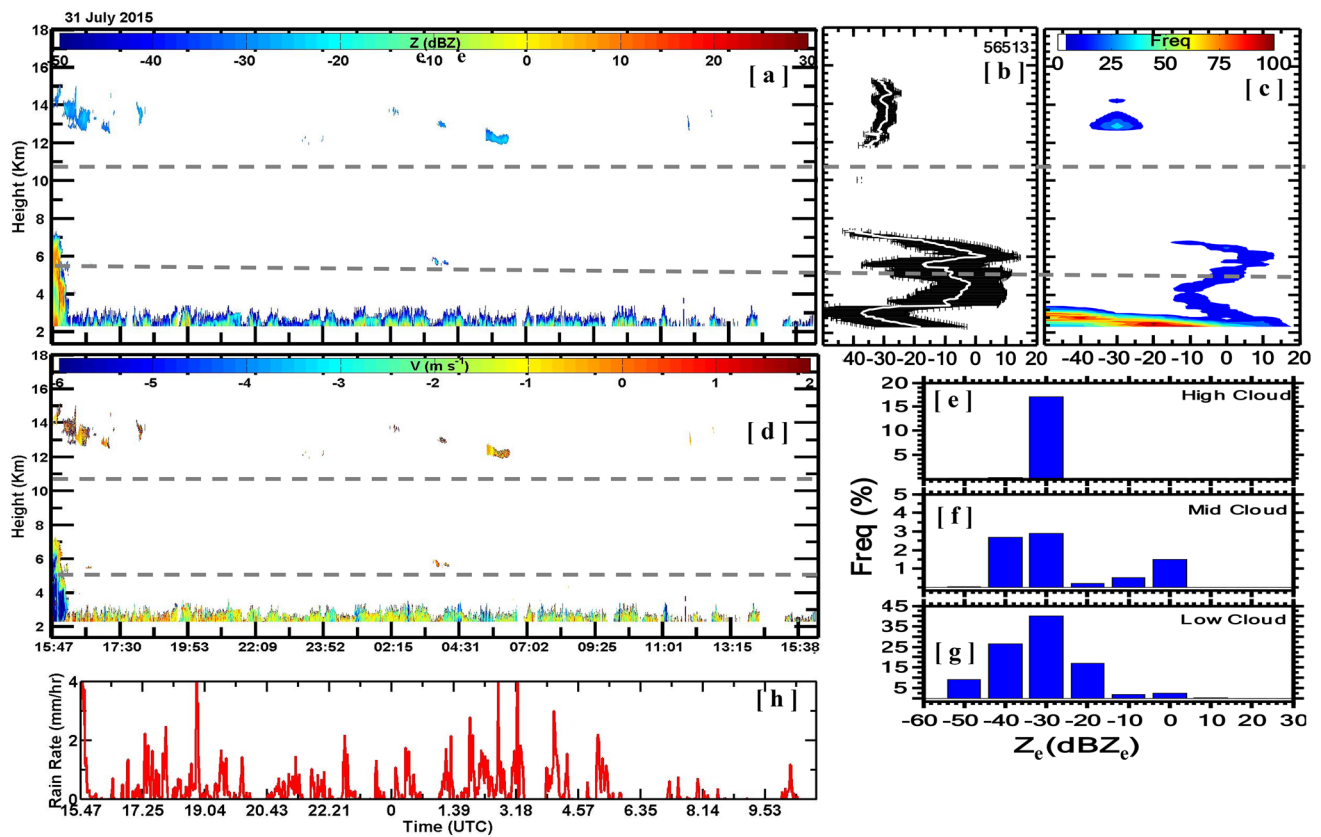
site as well as over the Arabian Sea, which further helps to sustain deep convective cloud.

Figure 4a, d show the HTI map of  $Z_e$  and V, which portrays the preponderance of shallow clouds whose heights restricted below 3 km level except during the initial conges-tus episode (around 15:47 IST). Daily mean VPR with the standard deviation also clearly shows a cloud-void zone at the mid-levels (Fig. 4b). Both mean VPR (Fig. 4b) and the CFAD (Fig. 4c) are contrastingly different from the active convective case on 09 Sep 2015 (Fig. 2). The negligible occurrence of clouds beyond 4 km AMSL is revealed from a meager 15% frequency count. CFAD analysis for 31 July 2015 (Fig. 4) does not show a linkage between the three different cloud phase regions, which contrasts with the previous case (Fig. 2). This typical broken structure of VPR is representative of the dry ISM day, where the variability of  $Z_e$  confines from  $-40$  to a maximum of  $10 \text{ dBZ}_e$ . There is no signature of rain as the maximum  $Z_e$  value  $\sim 10 \text{ dBZ}_e$  indicates only drizzling conditions. Figure 4e–g confirms the predominance of weaker clouds having a  $Z_e$  value of  $-30 \text{ dBZ}_e$  at all three clouds. These weak, shallow clouds further indicate the absence of strong convection beyond a 3 km level on the day. The rainfall continues throughout the day but restricted mostly below  $2 \text{ mm h}^{-1}$  (Fig. 4h), unlike the previous case (Fig. 2h). Due to the formation of intense low-pressure zones over the head Bay of Bengal and the northwest part of India, which can be visualized from weather maps from the IMD daily weather report in Fig. 5a, the dry condition persists over radar site. In Fig. 5b, RH profile also depicts similar information, where it starts decreasing from the surface and reaches a minimum value of 30% at 3.6 km AMSL and less than 60% in the mid-level (barring at fewer levels). Closely spaced isobars in Fig. 5a indicate the high wind speed over radar site. Detailed wind information is evident in Fig. 5c, which reveals the presence of low level ( $< 3 \text{ km AMSL}$ ) high speed, southwesterly but feeble wind speed at the mid-level (marked by a square box). Weak southwesterly maintains dry condition at the mid-level, restricting the growth of those clouds below 3 km AMSL. The horizontal cross-section of RH at 850 and 750 hPa in Fig. 5d, e shows cyclonic circulation over the Bay of Bengal and Rajasthan, indicating the increment of moisture over those regions at the expense of less humidity over the Arabian Sea and west coast of India.

Figure 5d, e depicts the advection of dry air from the northwest dessert part of India at the mid-troposphere, which results in dryness that region. Hence, due to the absence of sufficient humidity, cloud heights are confined below 3 km AMSL for most of the hours during that day despite having stronger winds at lower levels. For the same reason, shallow cloud formation and dissipation rates are persistent, which is the evidence from the erratic cloud boundary in Fig. 4a. The ice cloud process occurs on 09 Sep 2015 (Fig. 2a, c) is another

**Fig. 3** **a** IMD daily weather chart, ERA-Interim, **b** vertical profile of RH, **c** horizontal wind direction, the horizontal component of wind with background RH, **d** 850 hPa, **e** 750 hPa on 9 Sep 2015. Two overlays dashed lines correspond to the altitude at 0° and  $-40^{\circ}\text{C}$  over the Western Ghats





**Fig. 4** Same as Fig. 2 but for a shallow convective cloud seen on 31 Jul 2015

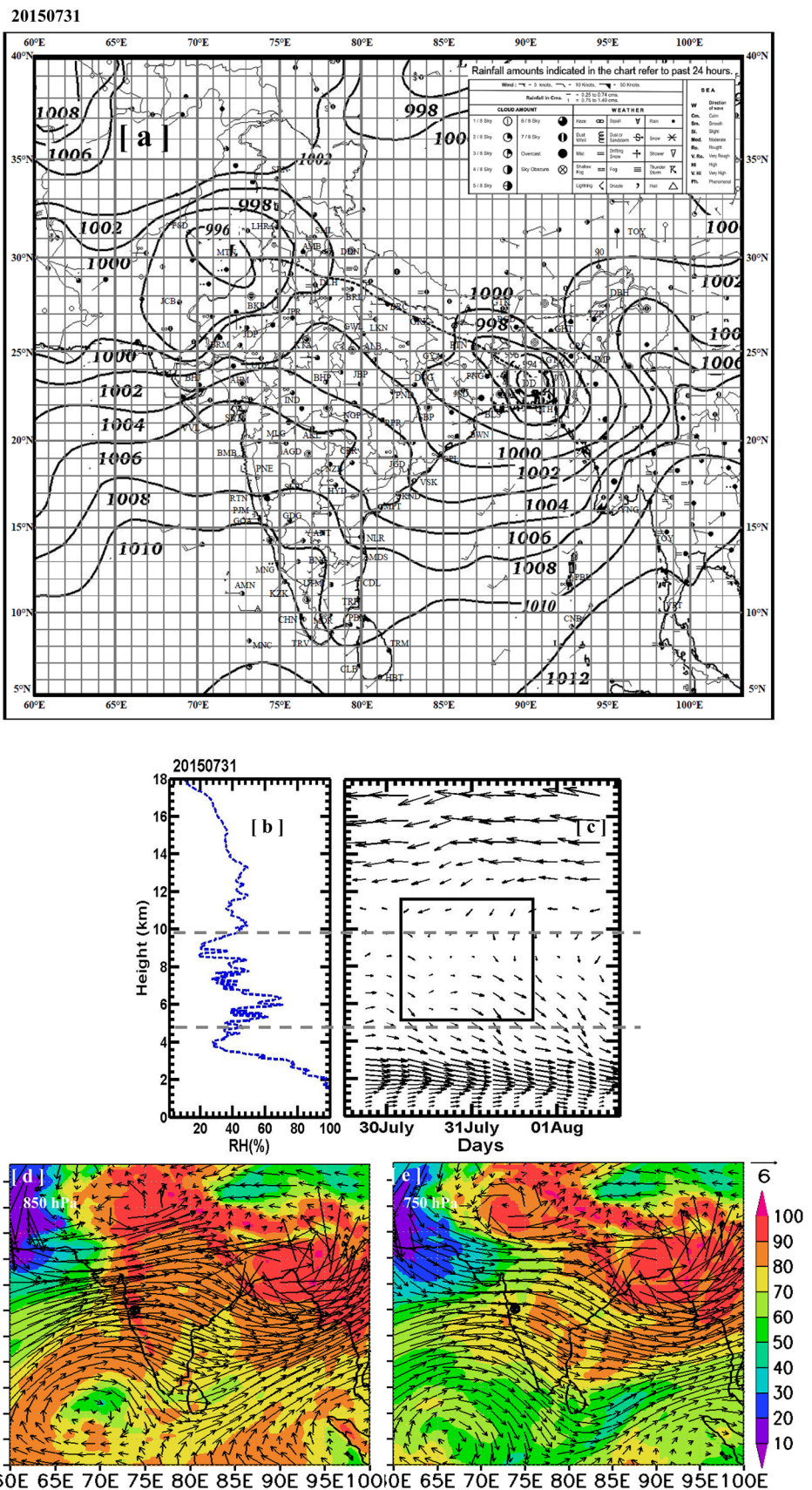
contrast to the warm rain process on 31 July 2015 (Fig. 4a, c). From the above two cases, it may be concluded that while deeper clouds herald maximum rain rates, continuous rainfall may well occur from shallow clouds with low rain rates over the WG.

The deep cloud and shallow cloud generation can also be explained in terms of the microphysical parameters i.e., ice water content and liquid water content, as found by Sukanya and Kalapureddy (2019). Their study explored CFAD analysis for 11 composite active and break ISM spells during 2014 using VPR to infer ice and liquid water content profiles. During ISM break days, LWC is limited below 3.5 km with a maximum occurrence of value  $0.1 \text{ g m}^{-3}$ . During ISM active days, the maximum existence of LWC is found to be  $1 \text{ g m}^{-3}$  reaching above 4 km. This difference in LWC leads to different cloud growth and hence, the contrast in VSC as discussed above.

#### 4 Cloud evolution during the two distinct background conditions

VSC is examined during two distinct atmospheric background conditions when low (Fig. 6) and high pressure (Fig. 8) systems prevail at close vicinity of the radar site, as confirmed in the synoptic charts of IMD daily weather report. For this purpose, VSC of two typical cases, among others such studied 5 cases representing those two conditions above have been analyzed here by the time evolution of VPR. Figure 6 is the same as that of Fig. 2 but for evolution confined to two consecutive days during 23–24 August 2014. Deep convection episode is for 20 min duration after 21 IST on 23 Aug whereas on 24 Aug the much vigorous convective events lasts longer period that exceeds more than 4 h. Deep convection during 24 Aug

**Fig. 5** Same as Fig. 3 but for 31 Jul 2015



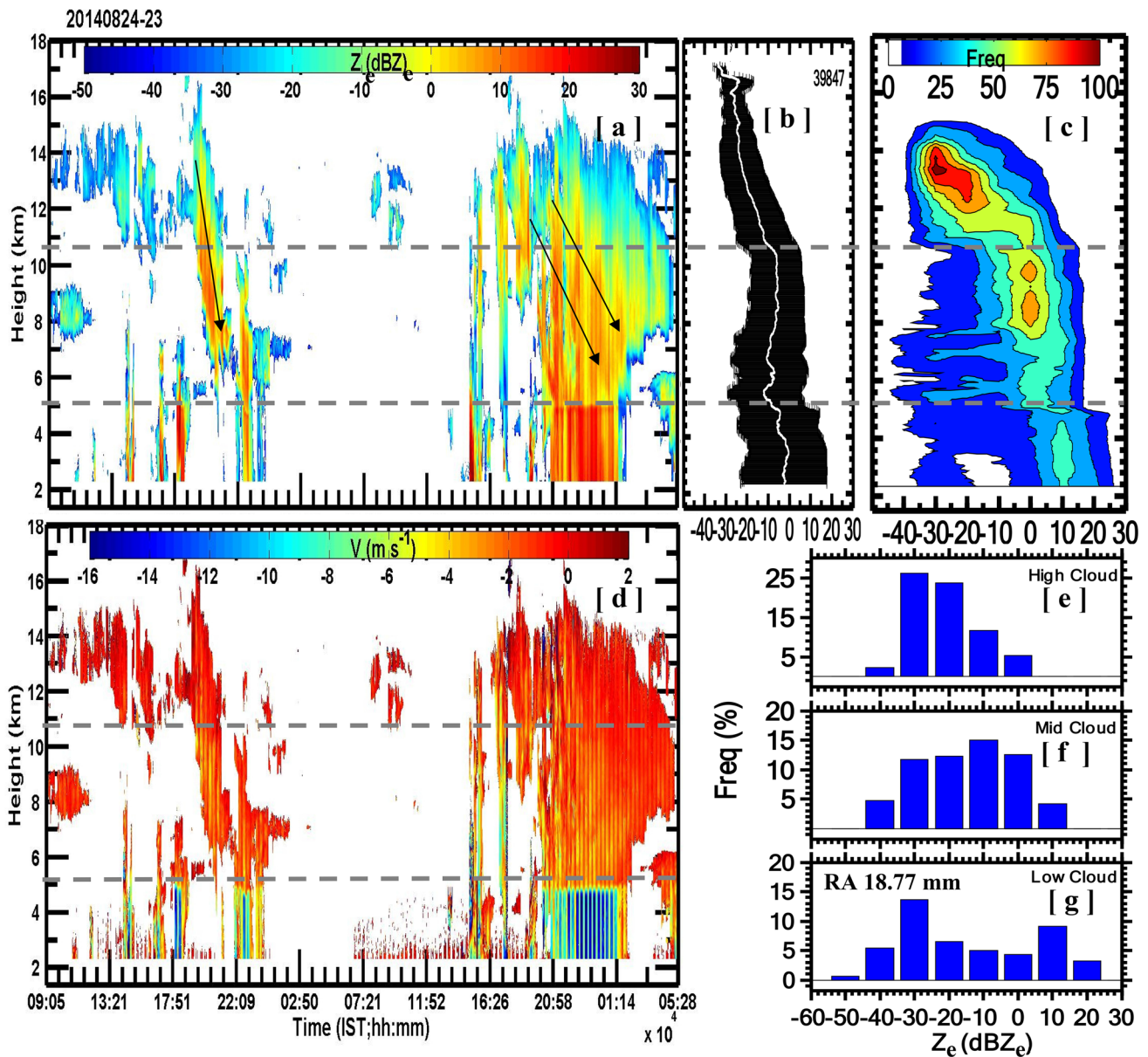
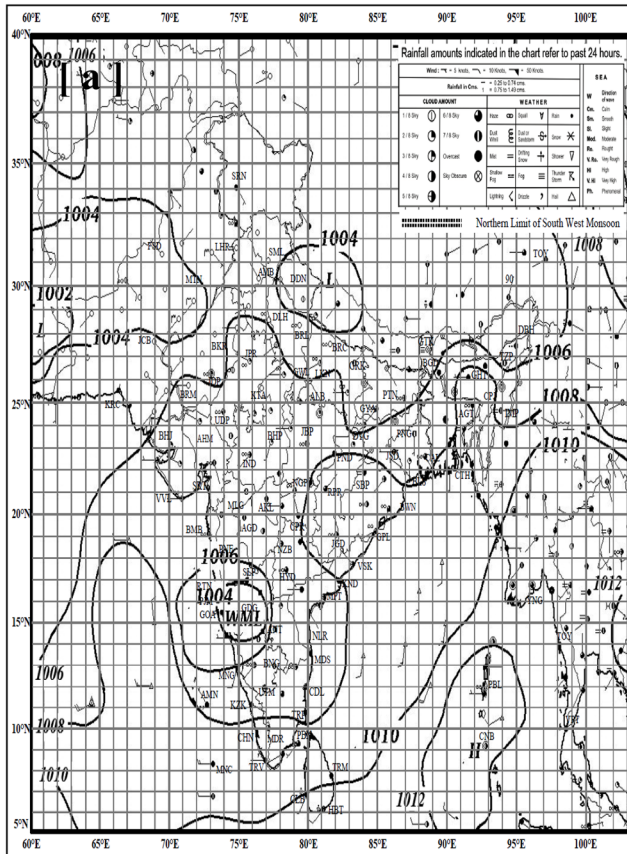


**Fig. 6** Same as Fig. 2 but cloud evolution under low-pressure conditions over the radar site during 23–24 Aug. 2014. The arrows indicate the path of bigger ice particles coming to the mixed-phase cloud region, evident from the increased  $Z_e$  value between the two areas

appears like an anvil cloud characterized by the spreading of cloud tops near the tropopause. Due to the presence of cyclonic circulation at the surface over the Arabian Sea coast (Fig. 7c), is an adequate moist wind flows over the radar site helping in the sustenance of deep convective clouds. This cyclonic motion at 750 hPa (Fig. 7d) indicates the adequacy of moisture nearly throughout the entire atmospheric column. Before the formation of the deep convection, the congestus cloud originates, moistening the mid-levels. During the first day (23 Aug 2014 in Fig. 6a), cirrus thickness increases with time in the afternoon hours and descends at a rate of  $0.5 \text{ km s}^{-1}$  (from 14

to 6 km within a span of 2 h 48 min. marked by an arrow in Fig. 6a). The occurrence of rain in the afternoon, evening, and night time is evident from the downward velocity value ( $> 8 \text{ m s}^{-1}$ ) in Fig. 6d when the drop size reaches 6 mm. The phase change region is prominent from the  $Z_e$  gradient in Fig. 6a around  $0^\circ$  isotherm. There is an abrupt change in velocity above the bright-band, which shows a velocity difference of a minimum  $5 \text{ m s}^{-1}$  between the falling ice particles to the water-coated ice particles falling below the bright-band. Presence of rainy cloud, both cumulus congestus and deep convective cloud (~40%) and a tiny amount of shallow cloud (cloud top < 3 km),

20140823



20140824

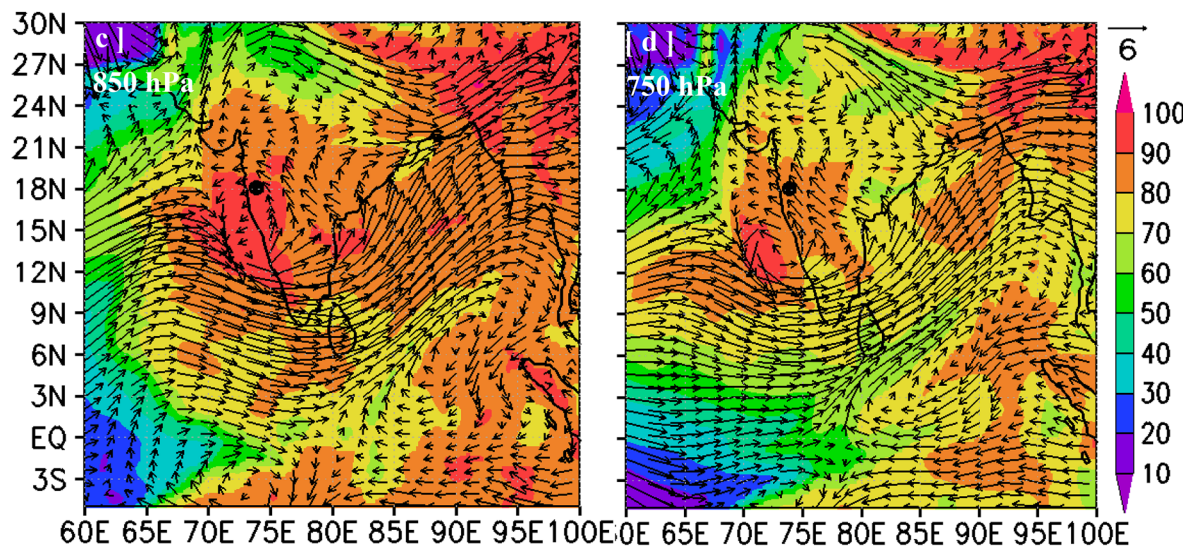
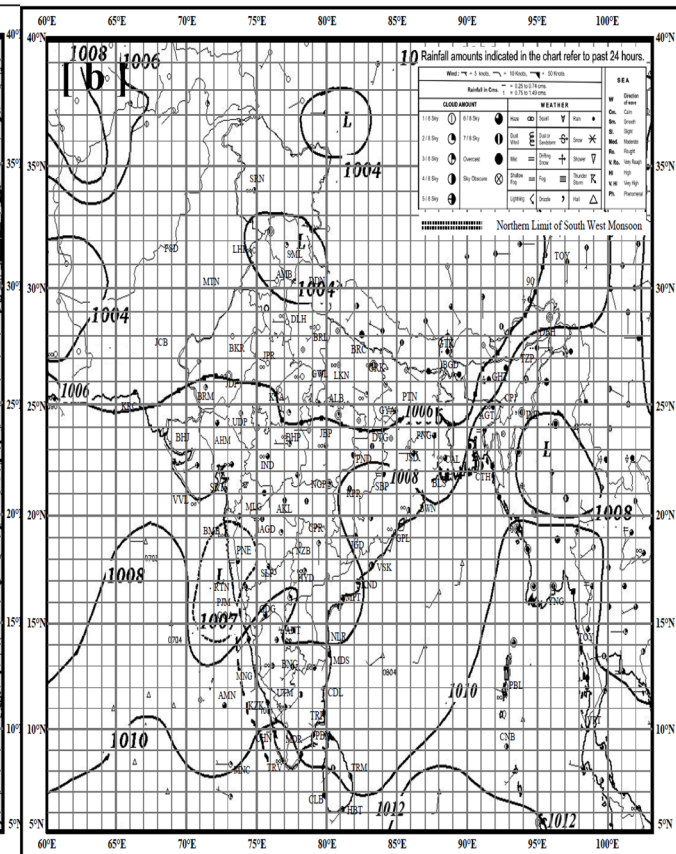


**Fig. 7** Daily weather chart of IMD for the **a** 23 Aug 2014 and **b** 24 Aug 2014 and ERA-Interim mean horizontal wind component with RH in the background for those two days at **c** 850 hPa and **d** 750 hPa

signifies strong convection indicative of persisting low-pressure system. A slanted line of high dBZ<sub>e</sub> (> 10 dBZ<sub>e</sub>) can be seen from high-level cloud towards mid-level cloud with the time progression around 19 h and lasts up to 01:14 h inside the deep convective cloud (arrow marked

in Fig. 6a). It indicates the initiation of bigger ice particles above 12 km, which slowly process down to the mid-level, which acts as feedback for rain from the ice phase to the mixed-phase particle and then liquid particles. This feature is prominently seen in the CFAD with Fig. 6c,

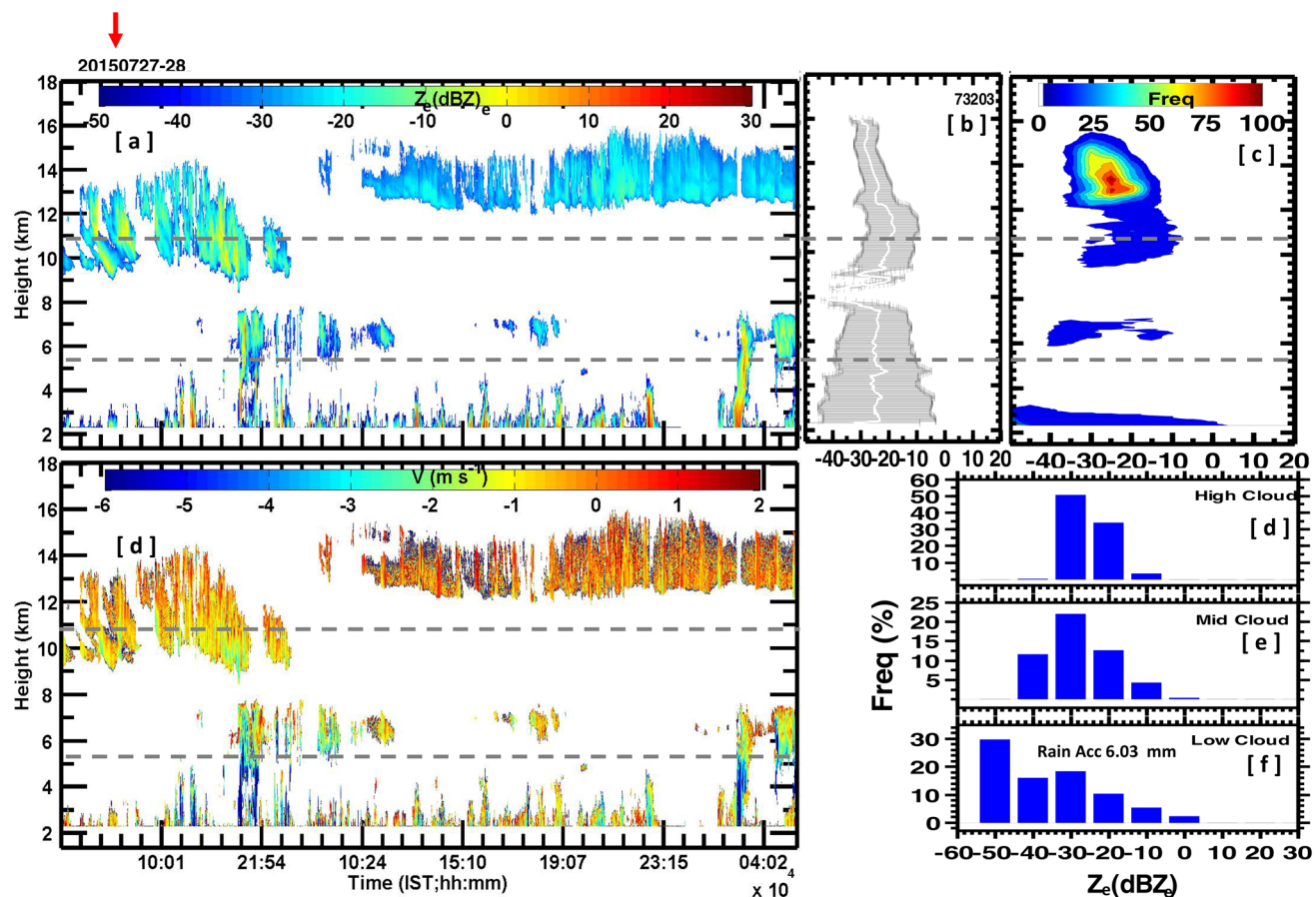


**Fig. 8** Same as Fig. 6 but for high-pressure conditions during 27–28 July 2015

which shows more than 50% (green contour) of the cloud particles get a transfer from the high- to mid-level, and almost 35% (cyan contour) of the cloud particles are linked from the ice- to warm-phase. The later have mean  $dBZ_e$  value around  $-10$  in the high-level and  $10$  in the mid- and low-levels, indicating that cloud particle growth leads to a rainy condition in the low-level. Weak, shallow non-precipitating clouds having mean  $dBZ_e = 30$  is present only less than 12% in the warm phase region.

Figure 8 carries out VSC's information during 27–28 July 2015, when high-pressure (1006 hPa and 1008 hPa) prevails in the close vicinity of the radar site confirmed from the (square box) IMD daily weather report in Fig. 9a, b, respectively. Due to the presence of a well-marked low-pressure system over Rajasthan and neighborhood, that converts into deep depression afterward. High-pressure condition prevails over the southwest part of India from 26 to 31 July 2015. Mainly shallow clouds whose top reach maximum up to 4 km dominate 90% of the time in these 2 days (Fig. 8a) with a small strip of congestus cloud, which ultimately splits into multilayered clouds. Rain accumulation for the present case is three times lesser than that of the earlier example

of 23–24 Aug 2014. Additionally, missing of deep convective cloud and meager presence of congestus clouds indicate these days are predominantly convectively inactive when high-pressure condition prevails. Due to the incidence of a cyclonic circulation over the Bay of Bengal and Rajasthan, a dense concentration of moisture can be seen only over those low-pressure system regions at the expense of humidity from adjoining areas like the Arabian Sea and associated coastal region. Though over radar site, RH is above 90% at the surface level in Fig. 9c, but it decreases with height, especially over the Arabian Sea at 750 hPa, as shown in Fig. 9d. Advection of dry air from the northwest part of India is also a possible reason for the mid-troposphere dehumidification. The rare presence of mid-level weak clouds also infers the fact of mid-level dry conditions. Unlike deep convective days, RH over the ocean is always below 80%. Due to the lesser rate of growth of ice particles, the cirrus cloud's descent can hardly be seen on the first day, whereas, on the second day, the growth rate is almost nil as the cirrus base is always above 12 km a uniform  $Z_e$  value around  $-10$   $dBZ_e$ . Figure 8b shows mean  $dBZ_e$  values are still less than  $-20$

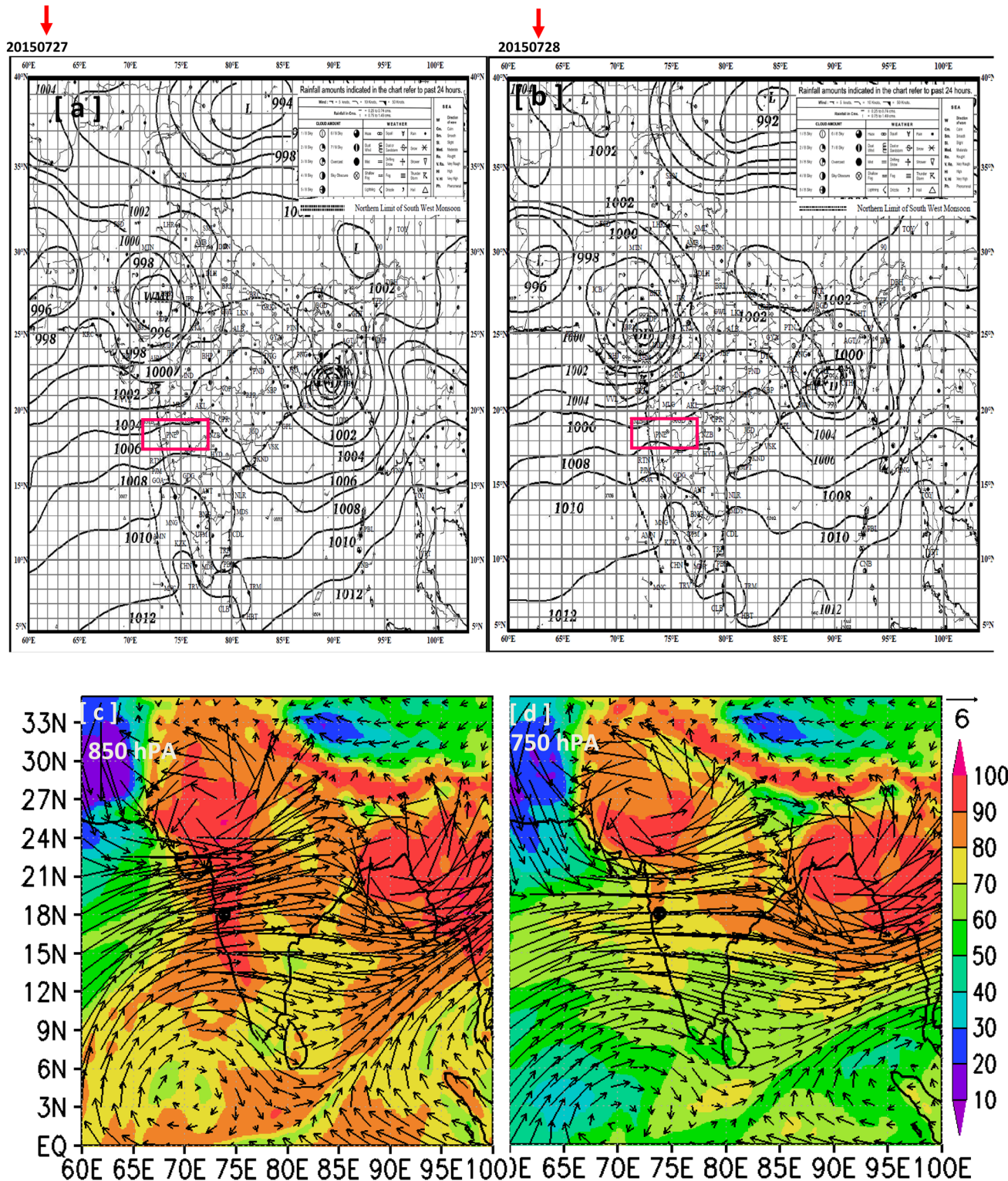


**Fig. 9** Same as Fig. 7 but for during 27–28 July 2015. The pink box represents the vicinity of the radar site where high pressure (1006 hPa) exists on 27 and 28 July 2015

on those 2 days, and maximum  $\text{dBZ}_e$  can reach only up to  $-5$ , limited at 2 km AMSL. CFAD analysis in Fig. 8c shows less than 25% of the total time low-level clouds were below 2 km AMSL. Increment of the frequency of occurrence can be seen for high-level clouds, but it is limited above 12 km AMSL. Unlike the earlier case, the link between ice phase cloud and mixed-phase cloud and mixed-phase cloud to warm phase cloud is missing. Though there was presence of cumulus congestus, their frequency is so less ( $>5\%$ ) that it's not captured in CFAD analysis resulting in less frequent or cloud void region in the mid-level. Figure 8d shows a dominance of weak downward velocity ( $<1 \text{ m s}^{-1}$ ), except during the presence of congestus cloud where maximum fall velocity reaches  $\sim 6 \text{ m s}^{-1}$ , which is half of the maximum speed observed in the previous case (Fig. 6d). It causes three times lesser rain accumulation in this case compared to the last case. The shift of cyclonic circulation from the Arabian Sea to the Bay of Bengal and Rajasthan causes the change in the source of humidity from the radar site, which inhibits the cloud growth above 4 km AMSL and also affected cloud particle size, compared to the previous case.

## 5 The transition of shallow to the deep cloud during ISM

The transition from shallow convection to congestus and then to the deep convective cloud is examined here to illustrate the congestus cloud's role for the onset of the deep convective cloud. For this purpose, the time evolution of VSC from July through August 2015 using half-hourly averaged VPR, and corresponding rain rate is shown in Fig. 10a, b, respectively. The grey dashed lines demarcate the three different cloud phase regions; warm, mixed, and ice clouds. For the first 18 days, shallow clouds with cloud top limited below 4 km AMSL are mainly dominating. Among those days, the absence of a cloud is also found in the warm phase cloud region marked by a grey circle in Fig. 10a. During those days, equivalent reflectivity factor value is less than  $-20 \text{ dBZ}_e$  indicating those shallow clouds are mainly non precipitating clouds. Cloud occurrence at the mid-level is almost unseen with the meager presence of thin and weak cirrus cloud for those same 18 days. After 18 days, cloud height starts increasing, with the increment in the equivalent reflectivity factor. The cumulus congestus cloud is explicitly seen from 19 to 22, 29–30 of Jul, as marked by grey dotted box in Fig. 10a with a maximum  $\text{dBZ}_e$  value of 10. At the same time, at high-level, cirrus activity also increases depicting from its consisting thickness and the maximum equivalent reflectivity factor value of  $10 \text{ dBZ}_e$ . Additionally, the descending feature in cirrus is evident with the increase of cirrus thickness. Here the cirrus base comes below 11 km. The increasing  $\text{dBZ}_e$  value and descending nature of the

cirrus cloud indicate the formation of bigger ice crystals, which glides down due to the ice sedimentation process beneath the cirrus cloud (Nair et al. 2012). Later, CC converts further into deep convective clouds (marked by a pink dotted box) whose cloud top reaches 14 km, and a maxima  $\text{dBZ}_e$  of 20 can be noted inside the deep cloud. Descending nature in the cirrus cloud can again be seen before the deep convective cloud occurs as the cloud base reaches below 8 km to merge with the low-level cloud. The merging of high- and low-level cloud by the descending nature of cirrus is again observed in the second episode of deep cloud day. Due to the smaller duration and less than  $-20 \text{ dBZ}_e$  reflectivity value at the ice phase region, convection is less intensive (maxima  $0 \text{ dBZ}_e$ ) than the previous deep cloud episode. Similar to earlier studies (Kemball-Cook and Weare 2001; Benedict and Randall 2007), the development of deep cloud is also evident hereafter the occurrence of congestus cloud, but this study deciphers the direct observational evidence for the first time. Generally, an average of a 5-day gap has identified between the formation of cumulus and deep convective cloud over the study region. Benedict and Randall (2007) explained that shallow cumulus and cumulus congestus help transport heat and moisture vertically, before the formation of deep convection. Hence, a subtle transformation of shallow to the deep cloud via CC and descending of cirrus can be seen in this paragraph. This feature is also associated with the transformation of non-precipitating to precipitating cloud indicated from the change of equivalent reflectivity factor from  $-25$  to  $20 \text{ dBZ}_e$ , which is also confirmed from the surface-based observation of IMD rainfall accumulation. Figure 10b shows that rain accumulation increases from shallow cloud day to the occurrence of CC and deep clouds. It is always below 5 mm on those days when shallow clouds are dominated. On the other hand, it is more than 5 mm when there is a presence of cumulus congestus and deep clouds. A rainfall maximum can be observed in the period between 27 and 29 Jul. Since humidity at the mid-troposphere has a significant effect on the development of the deep convection, here mid-level moistening has been taken place before the occurrence of deep clouds by these three processes (1) low-level convergence and formation of cumulus congestus which transport moisture from low- to mid-level, (2) cirrus descending from high- to mid-level, (3) horizontal moisture advection. The first two processes are well evident from the radar observed VSC. Large scale specific humidity and horizontal wind component have been utilized next to explore the third mechanism.

The reason behind the transition of shallow cloud to cumulus congestus, and then cumulus to subsequently deep cloud, is investigated from the large scale dynamical circulation response during the entire July and August 2015 reviewed in Figs. 11 and 12. HTI plot of RH profile from GPS-RS and ERA data (with horizontal wind direction) are

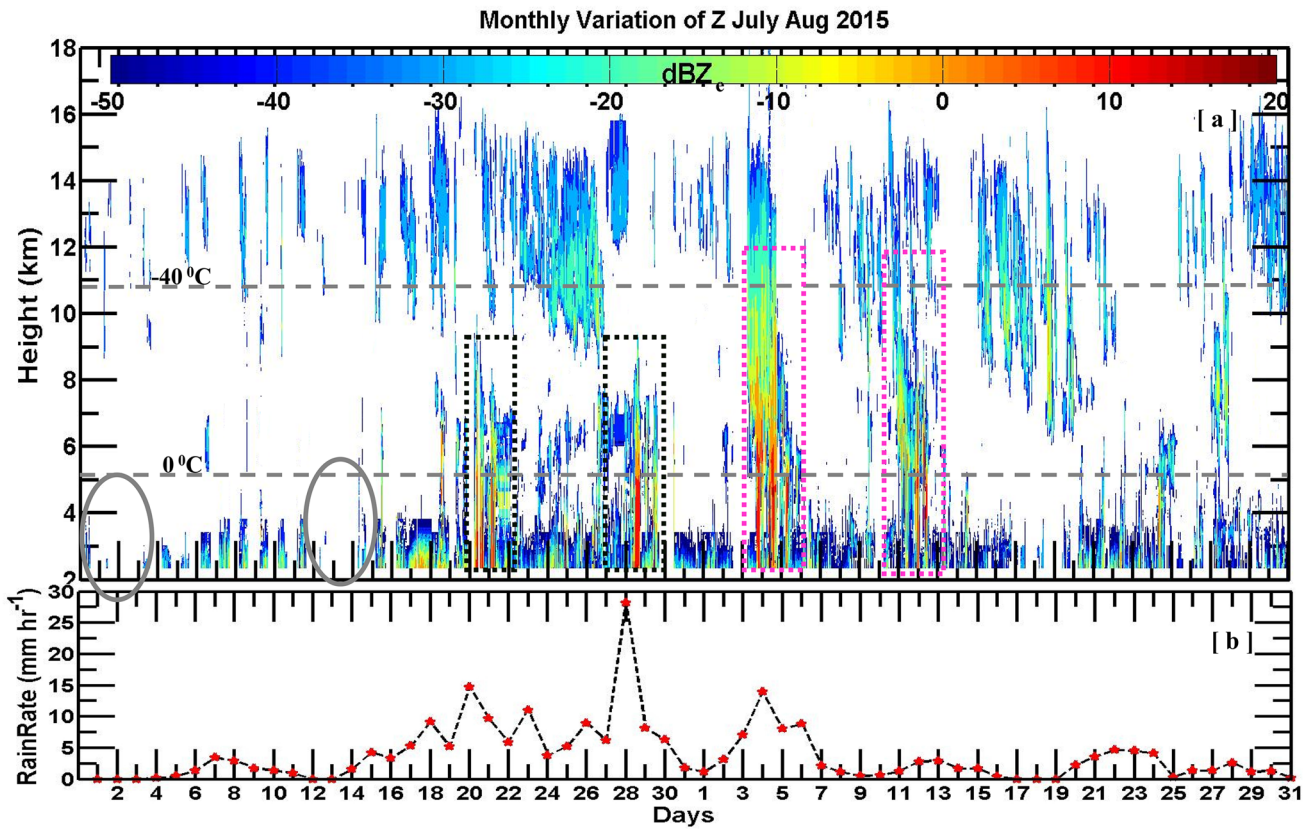


**Fig. 10** Evolution of VSC for July and August 2015 using **a** hourly averaged VPR and **b** IMD daily rainfall accumulation. Two overlay horizontal dashed lines correspond to the altitude at  $0^{\circ}$  and  $-40^{\circ}\text{C}$

over the Western Ghats. The black and magenta dotted boxes indicate the occurrence of CC and deep clouds, whereas, grey solid circles point the day with no cloud occurrence at low-level

shown in Fig. 11a, b, respectively. Mid troposphere dry conditions with the high CAPE value during the initial 18 days favor shallow cloud conversion into cumulus congestus (Khouider et al. 2010) can be seen from 18 to 21 Jul 2015. Since CAPE is proportional to the vertical velocity, updraft inside the cloud indicates a higher value of CAPE. Updraft more than  $1 \text{ m s}^{-1}$  of the cloud particles before and during the CC is confirmed from the radial velocity measurements of KaSPR (not shown). Whenever a congestus cloud formed over the radar site, mid-level humidity value started increasing to 80% after 20 July, as shown in Fig. 11a. It showed the upward transport of moisture from the boundary into the free troposphere preconditions the atmosphere for deep convection (Kemball-Cook and Weare 2001). This mid-level humidity reaches up to 80% just before the day of occurrence of deep cloud (grey box, Fig. 11b). With the mid-level moistening, the whole column maintains RH value  $> 80\%$ , as marked by red dotted square lines in Fig. 11a. Mid tropospheric moistening seen during 04–05 Aug (Fig. 11b) favors deep convection from cumulus congestus (Khouider et al. 2010). This high cloud height could explain continuous VSC with VPR on those days (Fig. 10a). On shallow cloud days, high RH value is limited only in the warm region below

3 km. Due to the presence of very little LWC ( $< 0.25 \text{ g m}^{-3}$ ), the shallow cloud is always less than 3 km (Sukanya and Kalapureddy 2019). In Fig. 11b, RH profile from ERA-interim is restricted up to 9 km for fidelity reasons beyond that height. In addition to RH, the horizontal wind component is a responsible factor for the transformation of clouds. This fact is evident by the RH exceeding 60%, whenever upper-level westerly wind alters into southerly or southwesterly, as shown by the square boxes in Fig. 11b, where shallow cloud converts into cumulus cloud and subsequently into the deep cloud. This change in the wind direction is very much prominent on the deep convective day when the entire column shows southerly wind, merging with the easterly wind below 3 km AMSL. Hence, it is concluded that humidity above 8 km AMSL is fed to the low level by the horizontal wind to help cloud development by making these levels rich in moisture. For the shallow cloud days, either RH less than 60% or the northerly wind component or the simultaneous presence of both, in the mid-level, ultimately opposes the easterly low-level seeding. It again confirms that both high humidity and southerly wind component in the 4–11 km level together act as feedback in the low-level to increase the cloud top height. Mid-level moistening is

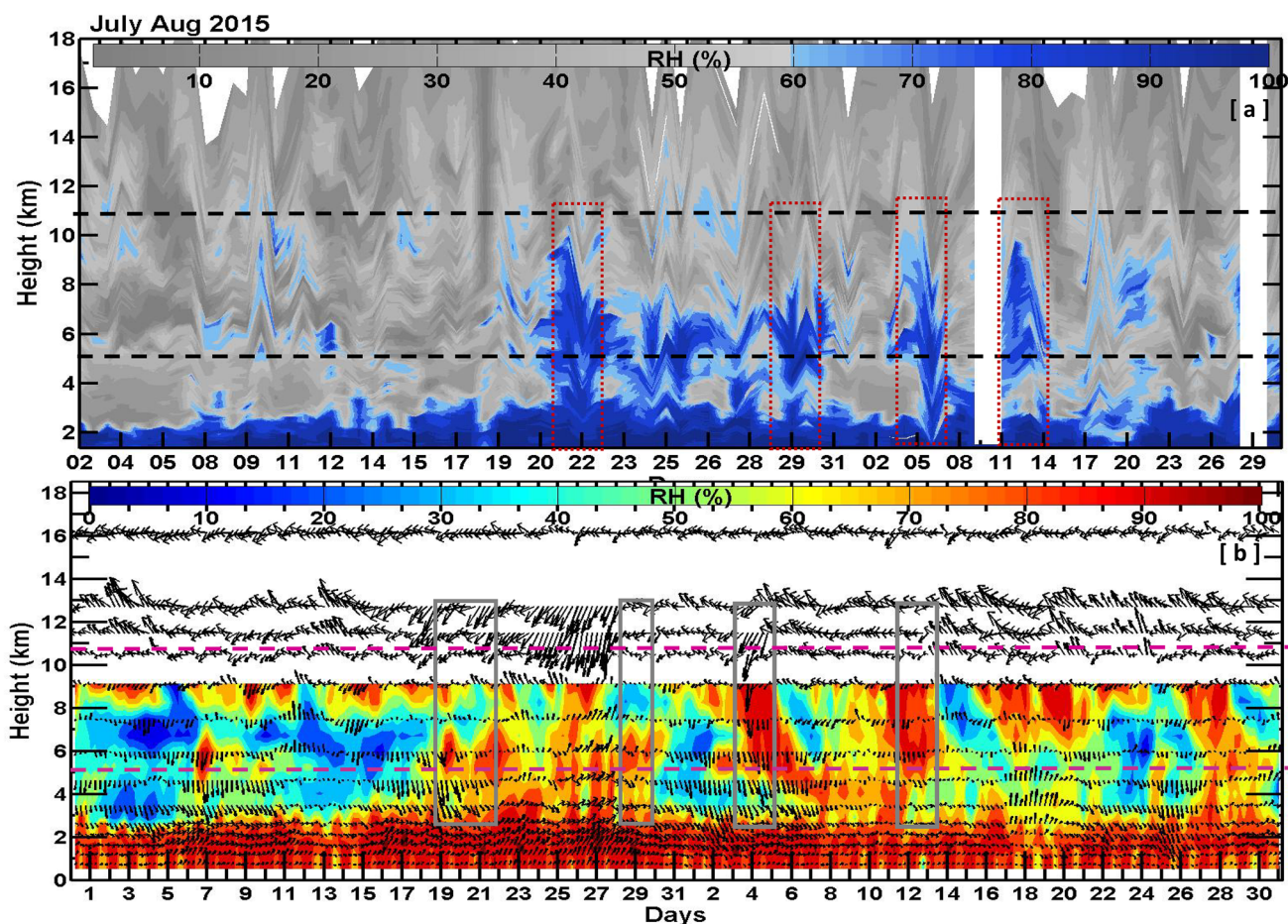


**Fig. 11** HTI plot of vertical profiles of **a** RH from Mahabaleshwar GPS-RS, and **b** RH with wind direction from ERA for July and August 2015. Mid-level moistening on the occurrence of CC and the

deep cloud can be seen by red dotted box and grey solid box in **a** and **b**, respectively. Two overlays dashed lines correspond to the altitude at 0° and  $-40^{\circ}\text{C}$  over the Western Ghats

initiated with cumulus congestus, and it becomes more prominent on deep convection days. In the first few days, horizontal moisture advection (Fig. 12a) shows negative values ( $< -1 \text{ kg kg}^{-1} \text{ s}^{-1}$ ), especially below 1 km, which indicates that horizontal transport of moisture becomes weak due to the weakening of the humidity carried by the southwesterly wind from the Arabian Sea. Another reason for the limited growth of the cloud is the dry air intrusion from the desert area in the northwestern part of India (Krishnamurti et al. 2010). This condition persists for the next 18 days, as shown by the purple dash-dotted box in Fig. 12a. During cumulus congestus, the positive value of horizontal moisture advection from the surface to 4 km AMSL (dark blue dotted box) represents the availability of sufficient moisture for cloud growth. Adveected moisture amount further increases around the day of deep convection (pink dotted box) as positive value sustains for a long time below 2 km AMSL with maximum from 2 to 3 km AMSL on the day of deep convection. Anomalous RH profiles also agree with the fact, as shown in Fig. 12b that mid-level anomalous RH increases

after 18 days and the whole column retains positive anomaly for 27–29 Jul 2015. No-cloud days are detectable by the RH anomaly profile as its showing negative RH anomaly in the low and mid-level ( $< -20\%$  and  $< -35\%$  respectively). Anomalous RH also shows abundant columnar humidity (blue dotted box) is responsible for rainfall maxima, whereas positive anomaly of RH ( $> 20\%$ , pink dotted box) is essential for cloud top height exceed 12 km as shown in Fig. 12b. This result agrees with the work of Del Genio et al. (2012) that shows during the suppressed phase of convection, there is a shallow cloud, and it is converted into a congestus cloud as the troposphere moistens and further it leads to widespread deep convection as column water vapor peaks.

FFT analysis has been performed in Fig. 13 for the JJAS time series of VPR with a median value of three range bins centered at 2.2, 3.2, 6.2, and 11.2 km altitudes correspond to AMSL, low-, mid- and high-level cloud region respectively associated with cloud vertical structure during 2014 and 2015. Figure 13 shows peaks in the amplitude between 5–10 days, 15–20 days, and at 30 and 60 days time period

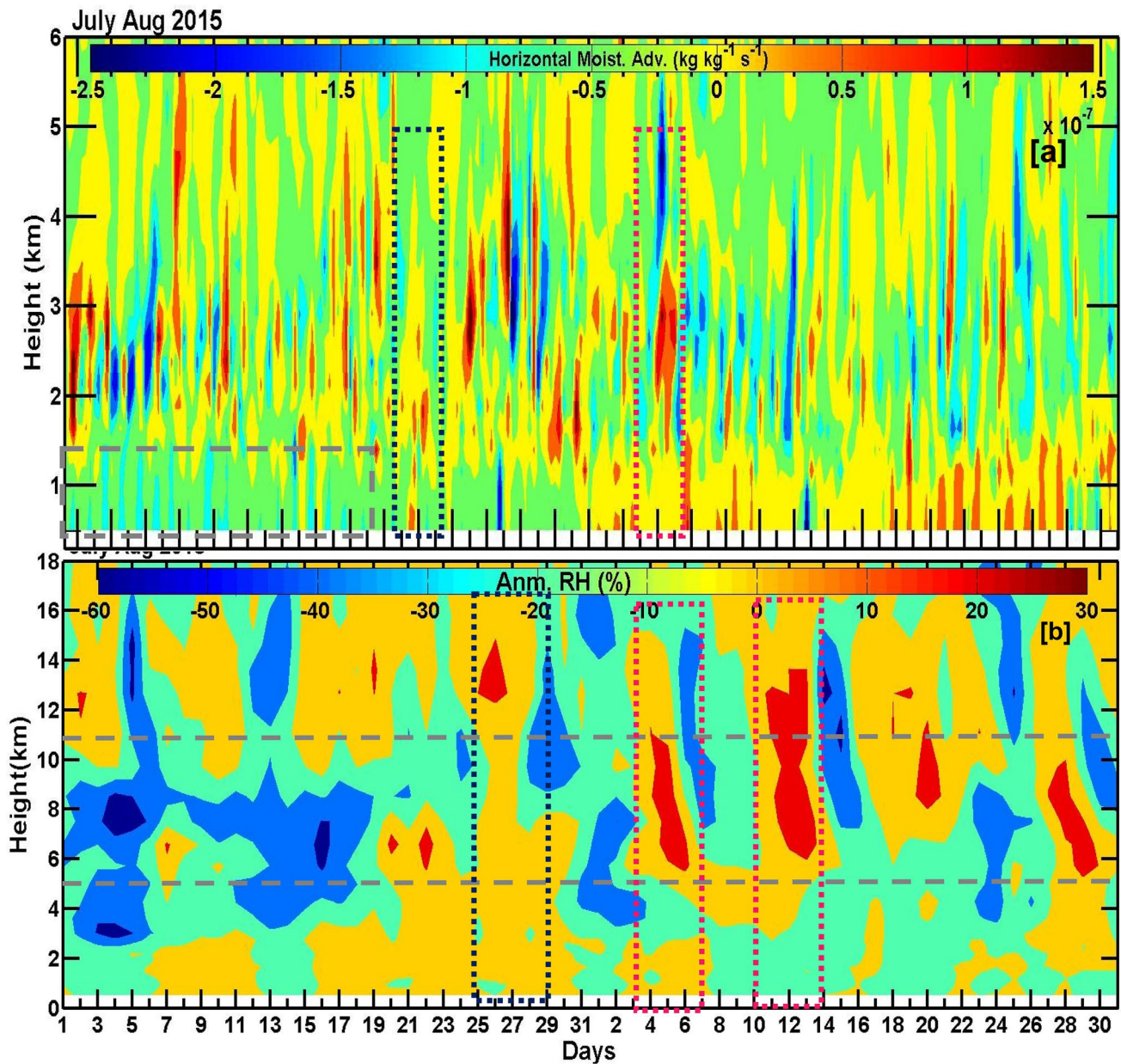


**Fig. 12** Vertical structure of ERA-Interim **a** horizontal moisture advection, grey dashed box shows the negative value, and increment in the horizontal moisture advection are shown by dotted boxes and **b** anomalous RH for July and August 2015. Two overlays dashed lines correspond to the altitude at 0° and  $-40^{\circ}\text{C}$  over the Western

Ghats. Anomalously humid conditions at the mid-level corresponds to the occurrence of deep cloud (magenta dotted boxes). The presence of adequate moisture in the whole atmospheric column (black dotted box) is observed on the day having maximum rain accumulation

existing for all the three cloud regimes for both the years. It indicates the dominance of those periodicities in the ISM season. Hence, the predominant intra-seasonal variability further can be inferred at 5–10, 10–20 to 30–60 day periodicities with year to year change of monsoon intraseasonal oscillation (MISO) features. Further, the north–south marching of tropical convergence zone leads to well known “active” and weak (or “break”) ISM spells that are characterized by heavy (wet) and deficit (dry) monsoon rainfall,

respectively. Previous studies have pointed out the importance of cloud vertical structure and cloud microphysics processes during active and break phases (Rajeevan et al. 2013; Dutta et al. 2020). The characteristic differences of cloud during the composite active and break ISM days are well evident over Mandhardev in WG (Sukanya and Kalapureddy 2019). Sukanya and Kalapureddy (2019) show the contrast in VSC during the composite wet and dry ISM spells by estimating and validating ice water content (IWC) and liquid

water content (LWC) using  $Z_e$  profiles from Ka-band radar. The significance of ice growth processes for heavy rainfall is prominent, which shows an order higher IWC value and greater thickness of ice clouds during active ISM spell. More than 66% of the concentration of IWC, even below 8 km (100% occurrence below 6 km) during active spell, suggests the enhanced IWC acts as a proxy for active ISM convection compared to break spell characterized by the complete absence of IWC features below 10 km. One order less LWC limited below 3.5 km during break spell explains cloud top inhibition below that height. Hence, VSC derived from cloud radar is a potential component for better understanding the active and break ISM spells besides MISO in terms of macro- and micro-physical cloud properties.

## 6 Seasonal cloud vertical structure during monsoon

### 6.1 Monthly mean VPR for inter- and intraseasonal ISM features during 2013–2015

VPR of monsoon months for 3 years suggests the differences in VSC associated with the various large scale monsoon background conditions and hence, rainfall variability. In Fig. 14 the VPR is averaged for each month around monsoon (MJSO for 2013, MJJA for 2014, JJAS for 2015) to delineate the monthly mean monsoon VSC for the year 2013–2015. As stated by the IMD monsoon report 2014 and 2015 are the deficit year in terms of rainfall for monsoon compared to monsoon 2013. Due to the favorable MJO activity, 2013 recorded heavy rain. On the contrary, the season rainfall of 2014 over the country was deficient, and this deficit broadened for monsoon 2015 (Kakatkar et al. 2018). This fact is also evident from the radar reflectivity profiles. For the

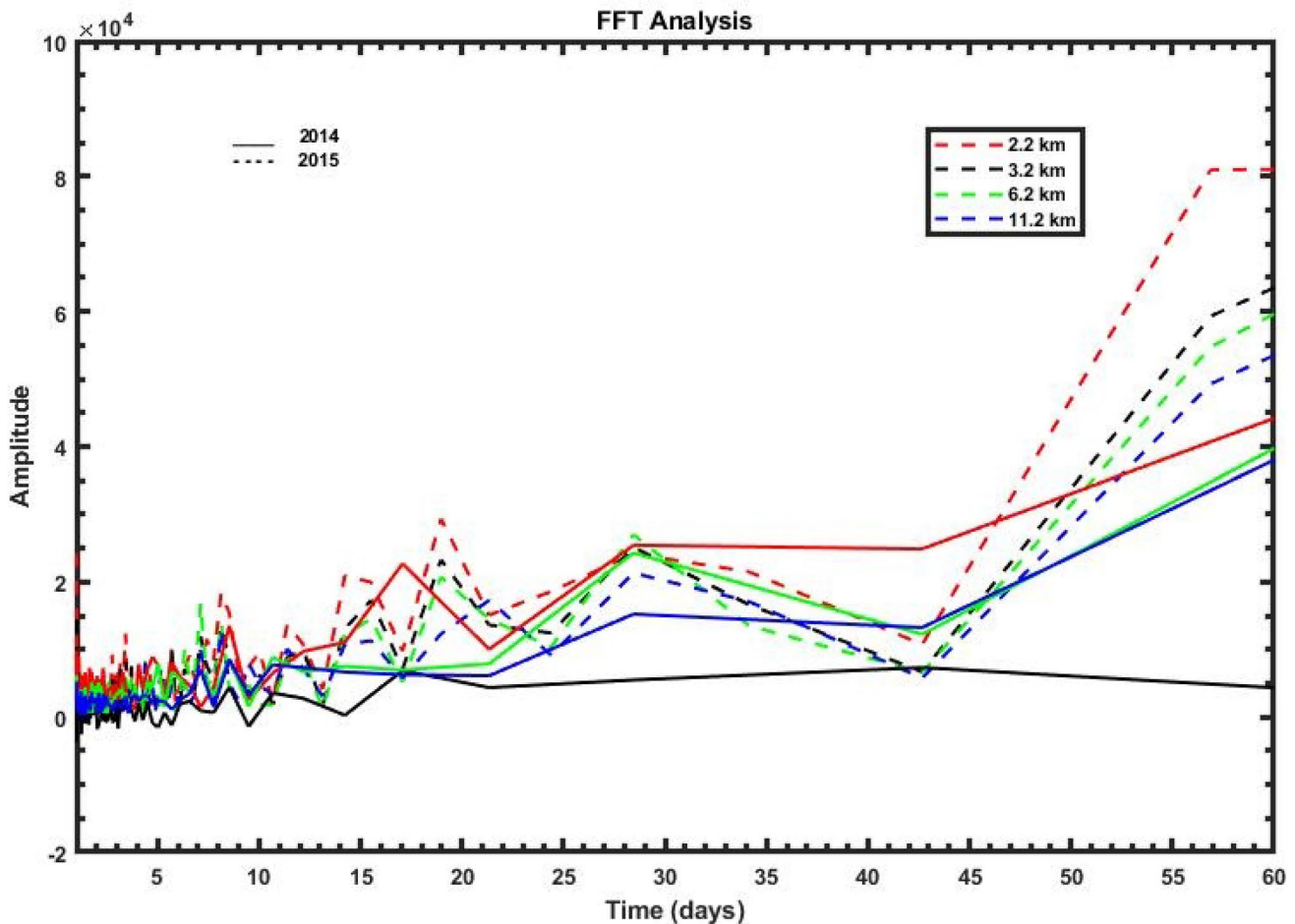


**Fig. 13** FFT analysis for the time series of VPR with a median value of three range bins centered at 2.2, 3.2, 6.2, and 11.2 km altitudes corresponds to AMSL, low-, mid- and high-level cloud respectively associated with cloud vertical structure during JJA 2014 and JJAS 2015

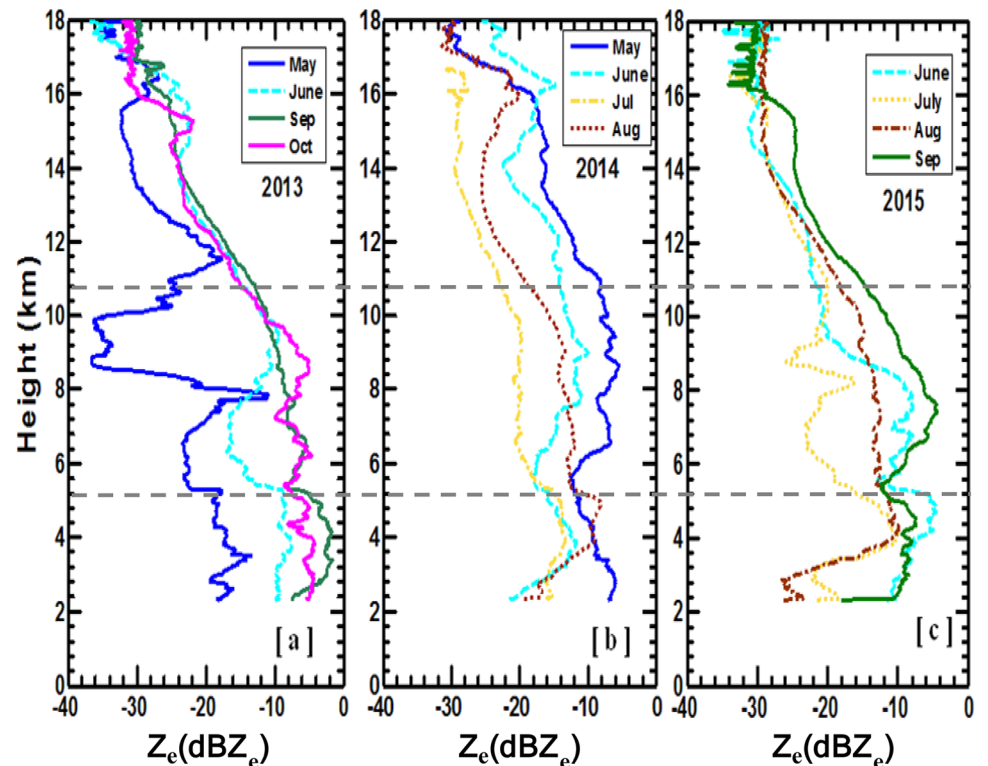
months of 2013, there is a gradual progression of  $Z_e$  values ( $\sim 10$ ) from pre-monsoon month (May) to monsoon months (Jun and Sep). The opposite trend follows in the next 2 years of 2014 and 2015, as shown in Fig. 14a, c, respectively, especially below 4 km; there is a sudden decrease in the  $dBZ_e$  values with decreasing height. Equivalent reflectivity factor value is reduced by  $\sim 10 dBZ_e$  in June 2014 below 3 km AMSL compared to that of 2013. All the three monsoon months (JJA) of 2014 show a lesser  $Z_e$  value around  $\sim -20 dBZ_e$  at the lowest range bin due to the domination of shallow non-precipitating cloud below 3 km. It ultimately results in a substantial deficiency in rainfall during June and the first half of July of 2014 due to the borderline El Niño and negative Indian Ocean dipole conditions, as stated by the IMD monsoon report. This report also says that there is a long spell of monsoon break in the middle of August caused by unfavorable phases of MJO. Except for July, the other three monsoon months show higher equivalent reflectivity factor value ( $\sim -10 dBZ_e$  or so) above 6 km, indicating deep convective clouds, which is also confirmed from Table 1. Due to the presence of dry conditions in the background atmosphere, the mid-tropospheric high  $dBZ_e$  values are not much helpful in making rain. Pre-monsoon convective activity due to the passage of western disturbances makes the  $dBZ_e$  profile of May 2014, laying above all the other profiles. El Niño conditions over the Pacific become strong in the middle of the season of 2015, which further degrades the  $dBZ_e$  value by  $\sim -6 dBZ_e$  in Jul and Aug compared to

2014 for the same 2 months. Though the  $dBZ_e$  profile of Sep between 2013 and 2015 is almost similar in terms of  $dBZ_e$  value, the difference in the number of deep convective clouds, rain accumulations are different, which is discussed in the next section. Interestingly, the overall trend of  $Z_e$  profile for each monsoon month remains the same, especially at the low level during the 3 years, but their  $Z_e$  values shift towards positive or negative depending on the large scale background condition.

## 6.2 Histogram analysis of VPR during three consecutive ISM seasons

Histogram analysis on VPR helps to inspect the annual variability of VSC by the normalized frequency distribution of  $Z_e$  for the three estate/level cloud regions; warm low-level, mixed mid-level, and ice phase high-level clouds. These three-level frequency distribution analyses also facilitate to understand the linkage among the three cloud regions. This section shows the role of low-level cloud distribution pertinent to the rain accumulation. Due to the TEST algorithm (Kalapureddy et al. 2018), the  $Z_e$  at the low-level cloud region can be considered to carry only meteorological cloud information. Figures 15, 16 and 17 shows monthly histogram analysis for 2013–2015, respectively. The number of profiles contributed for each month is specified at the top along with the monthly rain accumulation value with low-level clouds. Though the total number of profiles representing

**Fig. 14** Monthly mean KaSPR  $Z_e$  profiles for **a** 2013, **b** 2014 and **c** 2015. Two overlays dashed lines correspond to the altitude at  $0^\circ$  and  $-40^\circ C$  over the Western Ghats



the total number of cloud occurrences was highest in May 2013, the presence of cloud in all three levels is lowest compared to the other three months, as shown in Fig. 15a–c. The maximum occurrence of the low cloud is seen only up to 7% in Fig. 15, with the corresponding weak  $\text{dBZ}_e$  value of  $-40 \text{ dBZ}_e$ . It indicates that most of the days were no-cloud days in that month, and whatever cloud was present was weak (drop size  $< 10 \mu\text{m}$ ) in nature. Figure 18a–c describes the RH profile, the anomaly of RH, and latent heating (LH) profile, for the months of 2013. In Fig. 18a RH profile shows less humidity during pre- and post-monsoon periods than the two monsoon months, June and September of 2013. Narrow heating profiles (Fig. 18c) during May 2013 and October 2013 show the meager presence of cloud for that month, which is also confirmed from Table 1. Table 1 clearly shows 68% and 70% of the total time there was a no-cloud presence, for May 2013, and October 2013. As confirmed from Table 1, due to the enhanced occurrence of congestus cloud in Jun 2013, anomalous RH, especially in the mid-level  $> 15\%$  in Jun than the other months. Though the heating profile of June 2013 shows the highest heating rate at the mid-level, probably due to the evaporative cooling at the surface level confirmed from the  $-ve$  value of latent heat, rain droplets start disappearing before reaching the ground. It further results in less accumulation of rain in the same month than that of Sep 2013. Because of the presence of cumulus congestus and deep convective clouds as confirmed from Table 1, the LH profile of June 2013 and September 2013 show two peaks around 3 km and 6 km

AMSL, respectively. Bimodal distribution in the warm cloud region during June 2013 and September 2013 (Fig. 15f, i) can be seen with secondary peaks at  $10 \text{ dBZ}_e$  and  $20 \text{ dBZ}_e$ , respectively, crossing 15% normalized occurrence frequency. These peaks indicate the dominance of 1 mm drops (drop number density: 10), further hints the occurrence of a rainy cloud. For Jun 2013, a maximum  $Z_e$  value reaches up to  $30 \text{ dBZ}_e$ , which represent heavy rain condition. Despite the reason mentioned above, due to the fewer of observations (total 185,921 profiles) available in June 2013, overall rain accumulation is less (Fig. 15f, i) on that month than in September 2013. Mixed phase cloud occurrence (Fig. 15h) is maximum in Sep 2013, which might be the reason for maximum rain accumulation on that month as mid-level clouds play an important role in producing rain (Cui et al. 2011). This fact is evident from Table 1, where the cumulus and deep convective cloud is more in Sep than the rest of the months of 2013. Though cumulus maximally occurs during June 2013, their mean Z indicates below light drizzling condition ( $Z_e < -10 \text{ dBZ}_e$ ), which causes Jun to witness the second-highest accumulate rainfall. In 2013, delayed withdrawal of monsoon results in convective activity in October, which is evident in Table 1 with 1.73% occurrence of deep cloud on that month. The two bars in the  $\text{dBZ}_e$  histogram (Fig. 15l) centered around  $10 \text{ dBZ}_e$ , and  $20 \text{ dBZ}_e$  is the resultant of the convective activity, indicating light drizzling and heavy drizzling condition.

May 2014 shows more pre-monsoon convective activity than during 2013, which causes a bimodal distribution of

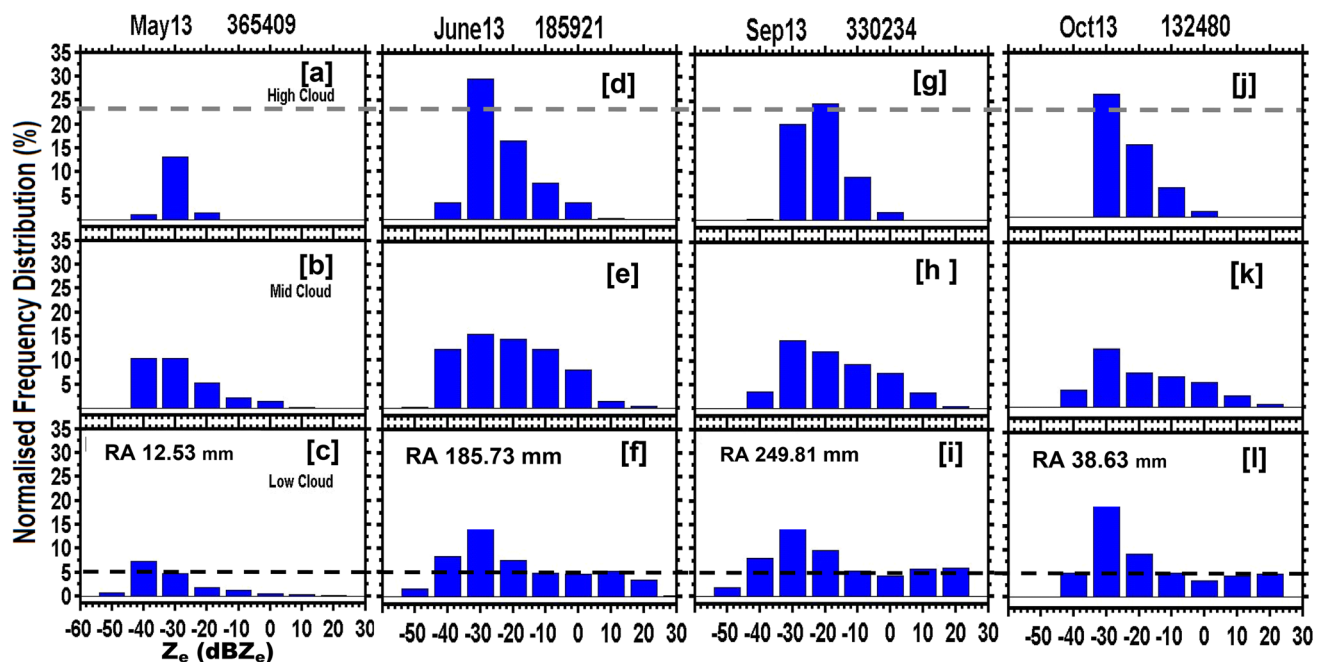


**Fig. 15** Normalized frequency distribution of three-level cloud equivalent reflectivity factor of **a–c** May, **d–f** June, **g–i** Sep. and **j–l** Oct. 2013. The number of profiles as labels and GPCP monthly rainfall accumulation is provided at the top at the bottom panels

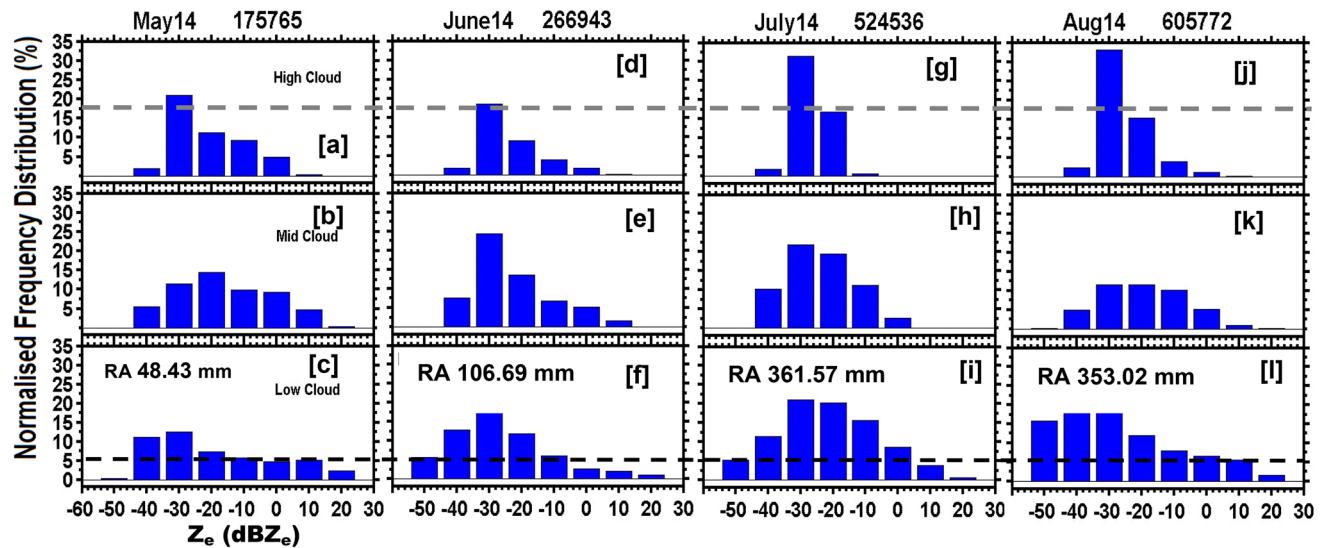


**Fig. 16** Same as Fig. 15 but for a–c May, d–f June, g–i July and j–l August of 2014

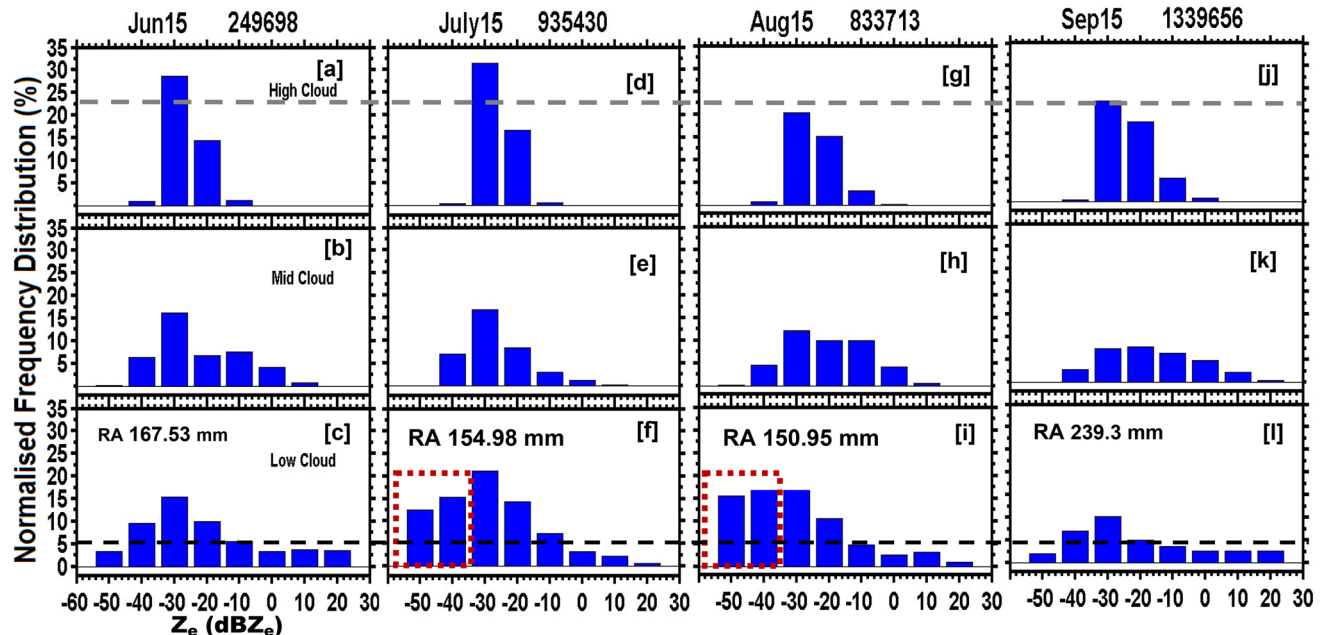


**Fig. 17** Same as Fig. 15 but for a–c June, d–f July, g–i August and j–l September of 2015. Two pink boxes are to show the enhanced non-precipitating clouds in July and Aug 2015

$\text{dBZ}_e$  in the low-level cloud (Fig. 16c) on that month. For the same month, in Fig. 19a RH value (blue curve) between 4 and 5 km also reaches as maximum as 80% (20% more than that of the previous month), and it is twice the value of the prior year at the high-level. An increase in the heating profile is also evident above 6 km in Fig. 19c. Unlike the last monsoon months, the trend of the bimodal distribution changes to mono-modal distribution for the monsoon months of 2014, which is shown in Fig. 16f, i, l. June has the lowest

amount of rain accumulation amongst these 4 months, where the number of profiles is also minimal compared to other monsoon months. The causative factor for June having the lowest rain accumulation is an anomalously moist ocean and coast with dry conditions over the land regions this month. Also, weak westerly with enriched humid conditions dominated over the windward side of the radar location (Utsav et al. 2017). In Fig. 19b negative and zero value of the RH anomaly (cyan curve) represent anomalously dry conditions

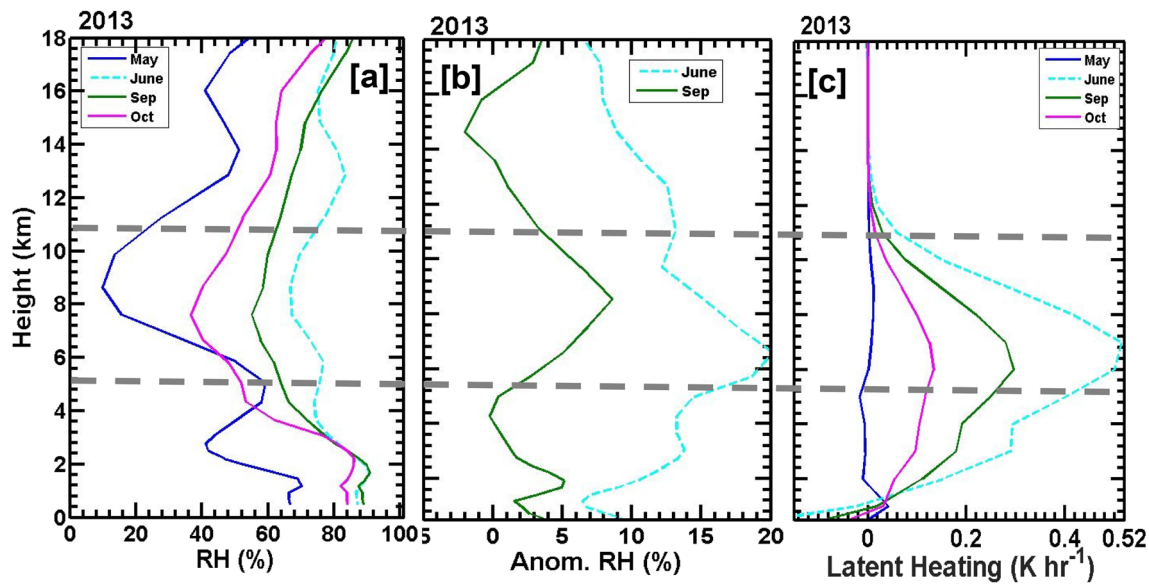


**Fig. 18** The ERA-Interim monthly average profile of **a** RH, **b** anomalous RH and **c** TRMM LH profile during 2013. Two overlays dashed lines correspond to the altitude at  $0^{\circ}$  and  $-40^{\circ}\text{C}$  over the Western Ghats

at the low- and mid-levels, respectively at a low level for June 2014. Due to this arid condition throughout the month, the occurrence of any type ( $Z_e \sim -10$  to  $20 \text{ dBZ}_e$ ) of precipitating clouds was minimum (below 2.5%) during June 2014. Though the maximum number of profiles is recorded during August 2014, they were dominated by the non-precipitating ( $-38 \text{ dBZ}_e$ ), shallow cloud, as evident from Table 1, where cloud occurrence below 3 km is 66% on that month. The maximum duration of cumulus congestus can be found in

July when mid-level cloud occurrence is also maximum (65%), as shown in Fig. 16h. It further results in maximum rain accumulation for that month, not only among the monsoon months of 2014 but also among the other 3 years. Due to CC with a deep convective cloud, two peaks can be seen at the low- and mid-level in the LH profile of July 2014. At the low-level, reflectivity distribution follows a Gaussian distribution in the warm cloud region in June and July with mean  $Z_e$  around  $-30 \text{ dBZ}_e$  and  $-20 \text{ dBZ}_e$ . So, it can be concluded

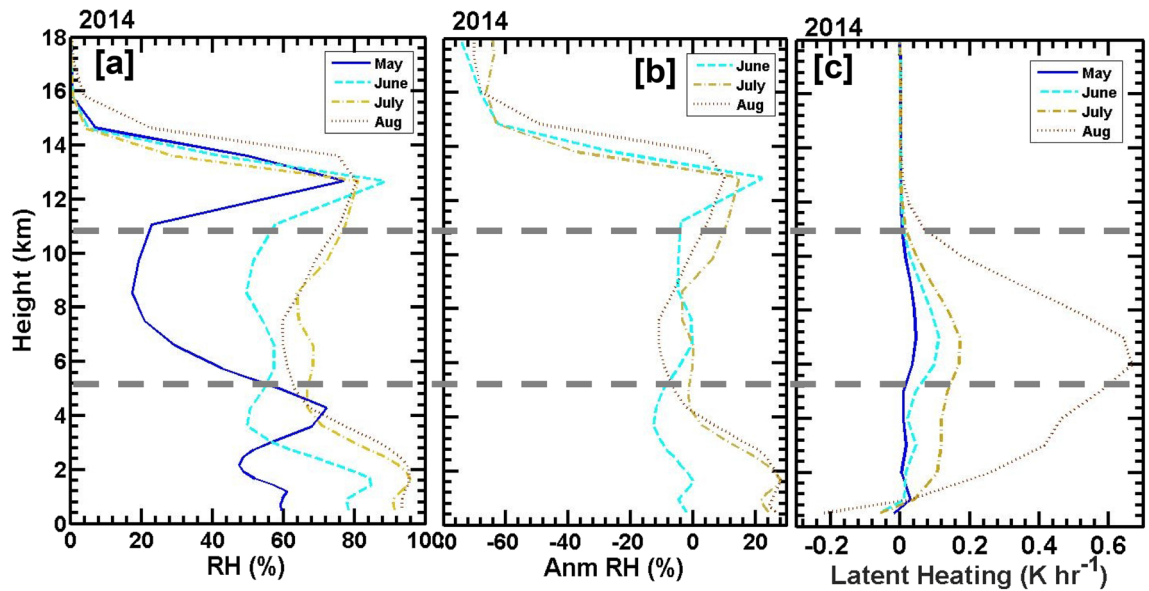


**Fig. 19** Same as Fig. 18 but for 2014

that non-precipitating clouds are more dominating in June and July of 2014. For August 2014, lognormal distribution can be seen at the warm phase cloud region skewed towards the negative values of  $Z_e$  in the distribution with greater than 10% occurrence of  $-50$  and  $-40$  dBZ<sub>e</sub> indicating the increase of the non rainy clouds compared to the previous two monsoon months again. In July, maximum rain accumulation is contributed by the drizzle as the equivalent reflectivity factor value of  $-10$  dBZ<sub>e</sub> exceeds 15%, highest among other months. In Fig. 19a, b, both July and August show same characteristics for RH and anomalous RH, but due to the low-level dryness signified by negative latent heating value at the surface in Fig. 19c, like June for 2013, rain accumulation is less in August than that of in July. Since cirrus clouds are the separated part from deep anvil cloud, duration of cirrus occurrence, and deep convective cloud, both are maximum for the same month August as evident from Table 1. Due to the maximum period of deep convective clouds in August 2014, this month shows a higher peak in latent heating profile compared to other months.

All the monsoon months of 2015 have a commonality in that all the cloud type distributions in the warm phase region are biased towards the smaller drops of size 0.01 mm when number density is  $10^{10}$  following log-normality. The distribution for precipitating regime ( $-10 \text{ dBZ}_e < Z_e < 30 \text{ dBZ}_e$ ) is always less than 5% except for Sep when the overall frequency count is very less at each region, as shown in Fig. 17. In both the primary monsoon months of Jul and Aug, the presence of non-precipitating cloud again increases, evident from the enhanced frequency of the lesser dBZ<sub>e</sub> value (dashed box in Fig. 17f, i) in the warm region. The reason is clear from Table 1, which shows the highest occurrences

of weak ( $\sim -35$ ) shallow cloud and less or no occurrence of deep cloud in those 2 months. A positive anomaly of RH below 3 km AMSL in Fig. 20b is seen only for June that causes maximum Z<sub>e</sub> ( $\sim 20$  dBZ<sub>e</sub>) for convective cloud among all 3 years. No-cloud days is maximum (65%) in June, due to the high latent heat release above 6 km AMSL in Fig. 20c on that month, intense convective clouds are much evident. It further causes the highest rain accumulation for June of that year. The dBZ<sub>e</sub> histogram also shows more frequency counts of precipitating clouds ( $\text{dBZ}_e > 10$  and  $\text{dBZ}_e > 20$ , respectively) in the warm region for the same month. Because of the presence of mid-level positive anomalous RH for September, deep convective clouds can sustain for a maximum time (6.52%) on that month compared to other monsoon months. Surface level dry condition is prominent from negative RH anomaly below 2 km AMSL in August and September, and hence, rain accumulation is less than that of June. The maximum duration of cumulus conges-tus (6.38% in Table 1) similar to previous years coincides with the maximum mid-level cloud occurrence in June. One common feature in all the 3 years is that irrespective of the background condition, 0.1 mm is the most dominating drop size among all the months and the entire three cloud region. Table 1 shows a subsequent increase in the occurrence of shallow clouds from 2013 to 2015, and the duration of Cc and deep cloud decreases severely, especially in the two primary monsoon months, July and August of 2015. Since Cc's occurrence plays a vital role in mid-level moistening and increment of rain accumulation, as established from Sect. 5, it can be concluded that a deficit or complete absence in the occurrence of Cc and deep cloud causes a deficit of rainfall on 2015 monsoon season. Though the appearance of cirrus

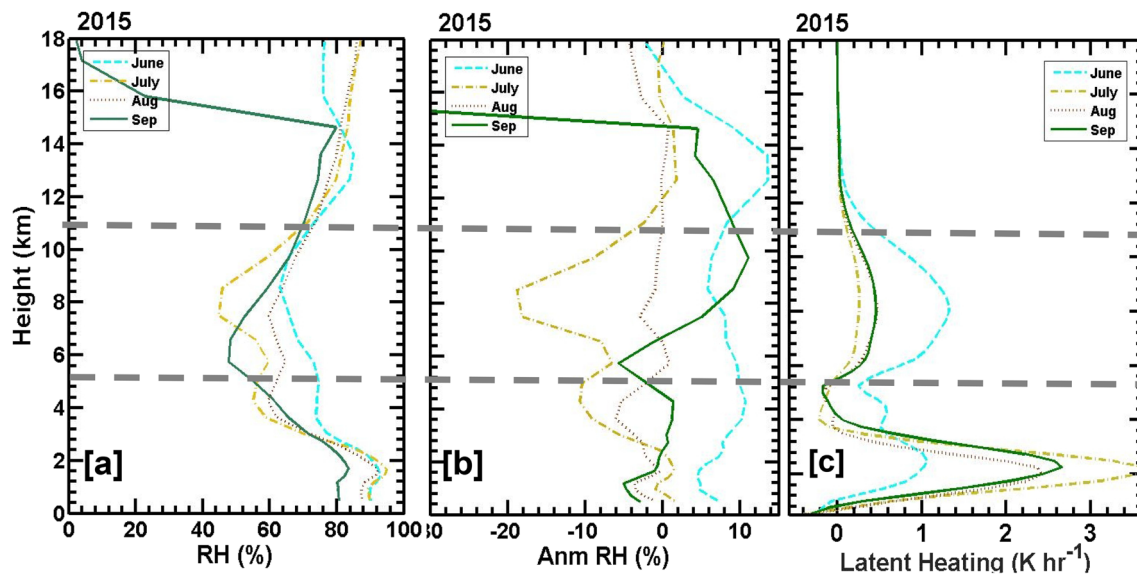


**Fig. 20** Same as Fig. 18 but for 2015

cloud increases during 2014 and 2015, but their mean  $Z_e$  value decreases, indicate the less activity of the ice growth process during those two seasons.

Further, the transition of shallow cloud to the deep convective cloud (Fig. 10) can be well understood by the latent heating profile of Jul and Aug 2015 (Fig. 20c). The vertical profile of latent heating (LH) peak in the mid-level cloud region indicates the release of latent heat due to the liquid to ice phase change above the freezing level. The latent heating in mid-level cloud regions invigorates the convection, causing a further rise in cloud tops height above 10 km altitude. This latent heating inside the cloud helps to grow the congestus into a deep convective cloud. However, the latent heat release externally accelerates the cloud dynamics by the improved updrafts from the cloud base due to the mid-level detrainment or sinking of air. LH in Fig. 20c shows a peak (green dashed curve) at the warm-phase cloud region for Jul 2015 due to the Cc's occurrence. For Aug 2015, due to the deep convective cloud, LH is more (dotted curve) at the mid-level than that of July 2015.

One of the essential observational evidence from the histogram analysis of VPR is the predominant cold cloud process contribution necessary to explain the higher monthly ISM rainfall yield (Figs. 15, 16). Whenever the monthly histogram of high-level ice cloud peck is exceeding above 22% of normalized frequency, which is evident to correlate with higher monthly rainfall accumulation, this cold cloud feature infers ISM higher rainfall involves a predominant cold rain process contribution.

## 7 Summary and conclusions

ISM intra-seasonal variability of tropical clouds is inspected using vertical looking high-resolution ground-based cloud radar VPR measurements in the height range of 0.9–16.7 km. The quality controlled cloud radar  $Z_e$  profiles infer the cloud macro-physical characteristics using the evolution of vertical structure of cloud (VSC) pertinent to a tropical Indian WG site during the ISM period. The VSC is a potential parameter to characterize the cloud at different time scales. The changes in the VSC are in response to both the local convection and large-scale ISM circulation. This remote sensing observational study investigates the daily to seasonal scale variability of ISM cloud vertical structure characteristics from 2013 to 2015 to infer the following conclusions:

1. On the deep convective day, the ice phase process contribution is prominent in producing rain as may be witnessed by an increment in the  $Z_e$  value in the ice phase region just before the increase in the rain rate at the surface. Whereas during a shallow cloud day, a meager

presence of cirrus cloud can be noticed with no signs of heavy drizzling.

2. A comparison of the two different days with the predominance of deep and shallower clouds shows that while deeper clouds herald maximum rain rates, continuous rainfall may well occur from shallow clouds with low rain rates. It may lead to near equal values in rain accumulation between the 2 days, despite the contrast in their VSC.
3. Cyclonic circulation generated over the coastal side adjoining the Arabian Sea is the primary source of moisture-rich flow at the low- and mid-level. The moisture-laden flow over the mid-levels especially helps in the profound cloud growth over the radar site. Contrastingly, a low-pressure system formed over Rajasthan and Bay of Bengal, creates deficient humidity over the WGs region, further causing shallow cloud growth.
4. Cumulus congestus has an essential role in mid-level moistening, which helps in the transition of shallow to the deep cloud, evident in the analysis of hourly average VPR data spanning over 60 days of the two consecutive ISM months. Both moisture advection and horizontal wind component are found responsible for this transition. The mid-level moistening is observed to be necessary for the growth and sustenance of the deep active ISM clouds.
5. The dominance of 15–20 days and 30–60 days periodicity are prominent in the FFT analysis of VPR for three cloud phase regions indicating the dominant role of MISO on VSC.
6. Annual variability of mean VPR can explain the change in rainfall signature based on the large-scale background monsoon conditions of that year.
7. The histogram analysis frequency distribution of  $\text{dB}Z_e$  at the low-level can address the dominance of precipitating and non-precipitating clouds according to the bi-modal and mono-modal distribution.
8. From 2013 to 2015, there is a subsequent increase of shallow cloud occurrence or no cloud regimes and a decrease in the presence of CC or deep cloud with the below normal performance of ISM.
9. VPR can associate the critical role of the cold cloud process for higher rainfall accumulation with consistent rainfall at the surface during the ISM months. Higher monthly rain accumulation during the ISM period mostly coincides with the dominance of high-level cloud frequency exceeding 22%.

Hence, it can be concluded that cyclonic circulation over the Arabian sea is the source of adequate moisture present at the mid-level over radar site, which causes the contrast in the cloud vertical structure, shallow to the deep cloud. Mid-level moistening by the occurrence of CC and generation of deep

cloud plays a vital role in the increment of the rainfall accumulation during monsoon. The purpose of ice phase processes at a high level also significantly crucial in producing heavy rain. One of the current VSC objectives is to decipher the climatologically meaningful information for the pragmatic representation of cloud in the coupled global models to improve the performance and reduce errors emanating from inadequate information on the cloud vertical structure.

**Acknowledgements** IITM is an autonomous organization that is fully funded by MOES, Govt. of India. Authors are grateful to Director, IITM, not only for his wholehearted support for strengthening the radar program but also for monitoring and acting as a source of inspiration to promote the radar research to the next heights. The authors are thankful to G. Pandithurai for encouraging discussions on the work and grateful to all those involved and helped in setting up and running the IITM's Cloud Radar Facility. The ERA-Interim data from the ECMWF (<https://apps.ecmwf.int/datasets/>). Authors also acknowledge Soumyajit Bose and Utsav Bhowmik for helping in analyzing massive radar and reanalysis data, respectively. The data supporting this article may be requested to the IITM radar data portal or corresponding author (kalapureddy1@gmail.com).

## References

- Benedict JJ, Randall DA (2007) Observed characteristics of the MJO relative to maximum rainfall. *J Atmos Sci* 64(7):2332–2354
- Brenguier JL, Wood R (2009) Observational strategies from the micro to mesoscale. In: Heintzenberg J, Charlson RJ (eds) *Clouds in the perturbed climate system: their relationship to energy balance, atmospheric dynamics, and precipitation*. MIT Press, Cambridge, pp 487–510
- Choudhury AD, Krishnan R, Ramarao MVS, Vellore R, Singh M, Mapes B (2018) A phenomenological paradigm for midtropospheric cyclogenesis in the Indian summer monsoon. *J Atmos Sci* 75(9):2931–2954
- Cui Z, Carslaw KS, Blyth AM (2011) The coupled effect of mid-tropospheric moisture and aerosol abundance on deep convective cloud dynamics and microphysics. *Atmosphere* 2(3):222–241
- Del Genio AD, Chen Y, Kim D, Yao MS (2012) The MJO transition from shallow to deep convection in CloudSat/CALIPSO data and GISS GCM simulations. *J Clim* 25(11):3755–3770
- Devasthale A, Fueglistaler S (2010) A climatological perspective of deep convection penetrating the TTL during the Indian summer monsoon from the AVHRR and MODIS instruments. *Atmos Chem Phys*. <https://doi.org/10.5194/acp-10-4573-2010>
- Devasthale A, Grassl H (2009) A daytime climatological distribution of high opaque ice cloud classes over the Indian summer monsoon region observed from 25-year AVHRR data. *Atmos Chem Phys* 9:4185–4196
- Dutta U, Chaudhari HS, Hazra A, Pokhrel S, Saha SK, Veeranjaneyulu C (2020) Role of convective and microphysical processes on the simulation of monsoon intraseasonal oscillation. *Clim Dyn* 55:2377–2403
- Francis PA, Gadgil S (2006) Intense rainfall events over the west coast of India. *Meteorol Atmos Phys* 94(1–4):27–42
- Gadgil S (2003) The Indian monsoon and its variability. *Annu Rev Earth Planet Sci* 31(1):429–467
- Gao W, Sui CH, Hu Z (2014) A study of macrophysical and microphysical properties of warm clouds over the Northern Hemisphere using CloudSat/CALIPSO data. *J Geophys Res Atmos* 119(6):3268–3280
- Goswami BN (2005) South Asian monsoon. In *Intraseasonal variability in the atmosphere-ocean climate system*. Springer, Berlin, pp 19–61
- Gunn R, Kinzer GD (1949) The terminal velocity of fall for water droplets in stagnant air. *J Meteor* 6(4):243–248
- Johnson RH, Rickenbach TM, Rutledge SA, Ciesielski PE, Schubert WH (1999) Trimodal characteristics of tropical convection. *J Clim* 12:2397
- Kakatkar R, Gnanaseelan C, Chowdary JS, Parekh A, Deepa JS (2018) Indian summer monsoon rainfall variability during 2014 and 2015 and associated Indo-Pacific upper ocean temperature patterns. *Theoret Appl Climatol* 131(3–4):1235–1247
- Kalapureddy MCR, Sukanya P, Das SK, Deshpande SM, Pandithurai G, Pazamany AL, Annam S (2018) A simple biota removal algorithm for 35 GHz cloud radar measurements. *Atmos Meas Tech*. <https://doi.org/10.5194/amt-11-1417-2018>
- KaSPR (2012) Calibration technical document prepared by ProSensing Inc., USA, (2012)
- Kemball-Cook SR, Weare BC (2001) The onset of convection in the Madden-Julian oscillation. *J Clim* 14(5):780–793
- Khouider B, Biello J, Majda AJ (2010) A stochastic multi-cloud model for tropical convection. *Commun Math Sci* 8(1):187–216
- Kollias P, Clothiaux EE, Miller MA, Albrecht BA, Stephens GL, Ackerman TP (2007) Millimeter-wavelength radars: new frontier in atmospheric cloud and precipitation research. *Bull Am Meteorol Soc* 88:1608
- Krishnamurti TN, Bhalme HN (1976) Oscillations of a monsoon system. Part I observational aspects. *J Atmos Sci* 33(10):1937–1954
- Krishnamurti TN, Thomas A, Simon A, Kumar V (2010) Desert air incursions, an overlooked aspect, for the dry spells of the Indian summer monsoon. *J Atmos Sci* 67(10):3423–3441
- Krishnan R, Zhang C, Sugi M (2000) Dynamics of breaks in the Indian summer monsoon. *J Atmos Sci* 57(9):1354–1372
- Liu C, Zipser EJ, Cecil DJ, Nesbitt SW, Sherwood S (2008) A cloud and precipitation feature database from nine years of TRMM observations. *J Appl Meteorol Climatol* 47(10):2712–2728
- Moncrieff MW, Waliser DE, Miller MJ, Shapiro MA, Asrar GR, Caughey J (2012) Multiscale convective organization and the YOTC virtual global field campaign. *Bull Am Meteorol Soc* 93(8):1171–1187
- Nair AKM, Rajeev K, Mishra MK, Thampi BV, Parameswaran K (2012) Multiyear lidar observations of the descending nature of tropical cirrus clouds. *J Geophys Res Atmos* 117:D18
- Rajeevan M, Rohini P, Kumar KN, Srinivasan J, Unnikrishnan CK (2013) A study of vertical cloud structure of the Indian summer monsoon using CloudSat data. *Clim Dyn* 40(3–4):637–650
- Randall DA, Dazlich DA, Corsetti TG (1989) Interactions among radiation, convection, and large-scale dynamics in a general circulation model. *J Atmos Sci* 46(13):1943–1970
- Rao YP (1976) Southwest monsoon, meteorological monograph. India Meteorological Department, New Delhi, p 366
- Romatschke U, Houze RA Jr (2011) Characteristics of precipitating convective systems in the South Asian monsoon. *J Meteorol*. <https://doi.org/10.1175/2010jhm1289.1American>
- Sassen K, Wang Z (2008) Classifying clouds around the globe with the CloudSat radar: 1-year of results. *Geophys Res Lett*. <https://doi.org/10.1029/2007gl032591>
- Sikka DR, Gadgil S (1980) On the maximum cloud zone and the ITCZ over Indian, longitudes during the southwest monsoon. *Mon Weather Rev* 108(11):1840–1853
- Slingo A, Slingo JM (1988) The response of a general circulation model to cloud longwave radiative forcing. I: Introduction and initial experiments. *Q J R Meteorol Soc* 114(482):1027–1062

- Stephens GL (2005) Cloud Feedbacks in the climate system: a critical review. *J Clim* 18(2):237–273
- Sukanya P, Kalapureddy MCR (2019) Cloud microphysical profile differences pertinent to monsoon phases: inferences from a cloud radar. *Meteorol Atmos Phys* 131(6):1723–1738. <https://doi.org/10.1007/s00703-019-00666-9>
- Tiedtke M (1989) A comprehensive mass flux scheme for cumulus parameterization for large scale models. American Meteorological Society, Boston
- Utsav B, Deshpande SM, Das SK, Pandithurai G (2017) Statistical characteristics of convective clouds over the Western Ghats derived from weather radar observations. *J Geophys Res: Atmos* 122(18):10050–10076
- Utsav B, Deshpande SM, Das SK, Pandithurai G, Niyogi D (2019) Observed vertical structure of convection during dry and wet summer monsoon epochs over the Western Ghats. *J Geophys Res Atmos* 124(3):1352–1369
- Wang J, Rossow WB, Zhang Y (2000) Cloud vertical structure and its variations from a 20-year global rawinsonde dataset. *J Clim* 13(17):3041–3056
- Webster PJ, Magaña VO, Palmer TN, Shukla J, Tomas RA, Yanai M, Yasunari T (1998) Monsoons: processes, predictability, and the prospects for prediction. *J Geophys Res* 103(C7):14451–14510
- Wielicki BA, Cess RD, King MD, Randall DA, Harrison EF (1995) Mission to planet Earth role of clouds and radiation in climate. *Bull Am Meteorol Soc* 76:2125

**Publisher's Note** Springer Nature remains neutral with regard to jurisdictional claims in published maps and institutional affiliations.